A quest for novel players in cardiac electrical function

Podliesna, S.S.

Publication date
2021

Chapter 3

Chronically elevated branched chain amino acid levels are pro-arrhythmic

Vincent Portero[*], Thomas Nicol[*], Svitlana Podliesna[*], Gerard A. Marchal, Antonius Baartscheer, Simona Casini, Rafik Tadros, Jorien L. Treur, Michael W.T. Tanck, I. Jane Cox, Fay Probert, Tertius A. Hough, Sara Falcone, Leander Beekman, Martina Müller-Nurasyid, Gabi Kastenmüller, Christian Gieger, Annette Peters, Stefan Kääb, Moritz F. Sinner, Andrew Blease, Arie O. Verkerk, Connie R. Bezzina[#], Paul K. Potter[#], Carol Ann Remme[#]

[*]These authors contributed equally to the study
[#]These authors jointly directed this work

Cardiovascular Research 2021 Jun 17;cvab207.
doi: 10.1093/cvr/cvab207.

ABSTRACT

Aim: Cardiac arrhythmias comprise a major health and economic burden and are associated with significant morbidity and mortality, including cardiac failure, stroke and sudden cardiac death (SCD). Development of efficient preventive and therapeutic strategies is hampered by incomplete knowledge of disease mechanisms and pathways. Our aim is to identify novel mechanisms underlying cardiac arrhythmia and SCD using an unbiased approach.

Methods and Results: We employed a phenotype-driven *N*-ethyl-*N*-nitrosourea (ENU) mutagenesis screen and identified a mouse line with a high incidence of sudden death at young age (6-9 weeks) in the absence of prior symptoms. Affected mice were found to be homozygous for the nonsense mutation *Bcat2*$^{p.Q300*/p.Q300*}$ in the *Bcat2* gene encoding branched chain amino acid transaminase 2. At the age of 4-5 weeks, *Bcat2*$^{p.Q300*/p.Q300*}$ mice displayed drastic increase of plasma levels of branch chain amino acids (BCAAs – leucine, isoleucine, valine) due to the incomplete catabolism of BCAAs, in addition to inducible arrhythmias *ex vivo* as well as cardiac conduction and repolarization disturbances. In line with these findings, plasma BCAA levels were positively correlated to ECG indices of conduction and repolarization in the German community-based KORA F4 Study. Isolated cardiomyocytes from *Bcat2*$^{p.Q300*/p.Q300*}$ mice revealed action potential (AP) prolongation, pro-arrhythmic events (early and late afterdepolarizations, triggered APs) and dysregulated calcium homeostasis. Incubation of human pluripotent stem cell-derived cardiomyocytes with elevated concentration of BCAAs induced similar calcium dysregulation and pro-arrhythmic events which were prevented by rapamycin, demonstrating the crucial involvement of mTOR pathway activation.

Conclusions: Our findings identify for the first time a causative link between elevated BCAAs and arrhythmia, which has implications for arrhythmogenesis in conditions associated with BCAA metabolism dysregulation such as diabetes, metabolic syndrome and heart failure.

Translational perspectives: Development of efficient anti-arrhythmic strategies is hampered by incomplete knowledge of disease mechanisms. Using an unbiased approach, we here identified for the first time a pro-arrhythmic effect of increased levels of branched chain amino acids (BCAAs). This is of particular relevance for conditions associated with BCAA dysregulation and increased arrhythmia risk, including heart failure, obesity and diabetes, as well as for athletes supplementing their diet with BCAAs. Such metabolic dysregulation is potentially modifiable through dietary interventions, paving the way for novel preventive strategies. Our findings furthermore identify mTOR inhibition as a potential anti-arrhythmic strategy in patients with metabolic syndrome.

Keywords: Arrhythmia; electrophysiology; sudden death; metabolism; BCAA

NON-STANDARD ABBREVIATIONS AND ACRONYMS

SCD	sudden cardiac death
ENU	*N*-ethyl-*N*-nitrosourea
BCAT2	branched chain amino acid transaminase 2
NMR	nuclear magnetic resonance
BCAA	branched chain amino acid
BCKA	branched chain ketoacid
BCKDC	branched-chain keto acid dehydrogenase complex
BCL	basic cycle length
hPSC-CM	human pluripotent stem cell-derived cardiomyocyte
AP	action potential
RMP	resting membrane potential
APA	action potential amplitude
APD	action potential duration
V_{max}	action potential upstroke velocity
EAD	early after depolarization
DAD	delayed after depolarization
TAP	triggered action potential
KORA	Cooperative Health Research in the Augsburg Region

INTRODUCTION

Cardiac arrhythmias comprise a major health and economic burden and are associated with significant morbidity and mortality, including cardiac failure, stroke and sudden cardiac death (SCD). SCD remains a leading cause of mortality in the Western world, accounting for up to 20% of all natural deaths, and up to 50% of all cardiovascular deaths.[1] Arrhythmias typically occur in the setting of an underlying pathology, including myocardial ischemia, structural derangements, and co-morbidities such as hypertension.[1,2] Furthermore, patients suffering from metabolic disorders (diabetes, obesity) and heart failure are at increased risk for arrhythmias and SCD.[3–8] Despite decades of research, few anti-arrhythmic therapeutic options exist due to the complexity of underlying pathologies. Development of efficient preventive and therapeutic strategies is essential but is as yet hampered by incomplete knowledge of disease mechanisms.

Over the last decade, we and others have employed several novel approaches to identify new disease mechanisms and pathways regulating cardiac electrical (dys) function, including genomic studies in rodents.[9,10] Phenotype driven screens have been very successful in identifying novel genes and alleles associated with disease, and resolving gene function.[11,12] In *N*-ethyl-*N*-nitrosourea (ENU) mutagenesis screens, pedigrees of mice with randomly induced point mutations are screened for a range of phenotypes and affected mice are subsequently used to map and clone the causative allele.[13] Employing such a phenotype-driven ENU screen, we here identified a mutant mouse line presenting with sudden death and a homozygous nonsense mutation in the *Bcat2* gene. Affected mice displayed a drastic increase of plasma branched chain amino acid (BCAA – valine, isoleucine, leucine) levels due to the incomplete catabolism of BCAAs, enhanced arrhythmia susceptibility, cardiac conduction and repolarization disturbances, and excessive pro-arrhythmic intracellular calcium dysregulation in isolated cardiomyocytes. In support of a role for BCAAs in modulation of cardiac electrical function, plasma BCAA levels were positively correlated to ECG indices of conduction and repolarization in individuals from the general population.[14] Studies in human pluripotent stem cell-derived cardiomyocytes furthermore confirmed a direct pro-arrhythmic effect of elevated BCAAs, and demonstrated the crucial involvement of the mammalian target of rapamycin (mTOR) activation in mediating these effects. Our findings thus demonstrate a causative link between elevated BCAAs and arrhythmia, which has implications for furthering our understanding of mechanisms underlying lethal arrhythmias, particularly those occurring in disease states associated with elevated BCAA levels such as diabetes and metabolic syndrome.[4–6,14–17]

MATERIALS AND METHODS

Mice

All animals were housed and maintained in the Mary Lyon Centre at MRC Harwell, under specific pathogen-free (SPF) conditions in individually ventilated cages, with environmental conditions as outlined in the Home Office Code of Practice. Home Office ethical approval was granted under project license 30/3070 and mice were euthanized by Home Office Schedule 1 methods. All experiments involving mice conformed to governmental and institutional guidelines for animal use in research and were performed with approval of the Animal Experimental Committee of the Academic Medical Center, Amsterdam (license AVD1180020184986). For ECG measurements, general anaesthesia was induced with 4.0% isoflurane and maintained at 0.8-1.2% isoflurane in oxygen. Euthanasia was performed by 100% CO_2 administration (20% v/v per minute), followed by cervical dislocation.

Generation of mutagenized pedigrees

The details of the ENU program have been described previously.[11] Briefly, C57BL/6J male mice (G_0) were treated with ENU doses of 1 x 120mg kg^{-1}, and then 2 x100mg $kg^{-1}$with a week between each dose. The mice were then bred with wild-type 'sighted C3H' (C3H.Pde6b+) females.[12] The resulting G_1 males were bred with wild-type C3H.Pde6b+ females to produce G_2 females, which were backcrossed to their G_1 fathers to generate G_3 offspring. The G_3 mating scheme results on average in 1 in 8 G_3 mice homozygous for any particular ENU-induced mutation. Binomial probability calculations indicate that a cohort of 50 single sex mice will yield 4 homozygotes with a probability of ~85% and 5 with a probability of ~75%. Initial identification of the sudden death phenotype was in G3 mice (batch A) but subsequent studies employed mice backcrossed ten generations to the C3H.Pde6b+ background (batch B). Measurements and experiments were performed in mice of either sex at the age of 4-5 weeks, unless otherwise specified (as further specified in the **Data Supplement**).

Mapping and DNA sequencing

DNA from affected mice and littermates was prepared from ear biopsies and used for linkage mapping utilizing the Illumina GoldenGate Mouse Medium Density Linkage Panel (Gen-Probe Life Sciences Ltd, UK). DNA from the founder G_1 mouse was prepared for whole genome sequencing (WGS) using the Nucleon BACC2 Genomic DNA Extraction System (GE Healthcare Life Sciences). After library generation, a single lane of paired-end sequencing (100nt) was performed employing the Illumina HiSeq platform (Oxford Genomics Centre, Wellcome Trust Centre for Human Genetics) and analyzed as previously described.[11] Genetic variants identified by WGS were confirmed by pyrosequencing (see **Data Supplement**).

NMR methodology and biochemical screen

Because of the severe nature of the phenotype and risk of early death, the phenotyping of this line was limited primarily to post mortem analysis. The function of the *Bcat2* gene suggested the possibility of abnormal levels of metabolites such as branched chain amino acids. To prevent the unnecessary death of mice, urine and plasma of male and female mice aged between 4 and 5 weeks of age was analysed by NMR. Details on urine and plasma sample preparation, NMR analysis, and estimation of the valine and xleucine (leucine and isoleucine combined) concentrations from the NMR spectra are provided in the **Data Supplement**. Further analysis of plasma was carried out by a clinical chemistry analysis of terminal plasma samples; further details are provided in the **Data Supplement** and **Suppl. Table S1**.

Western blot analysis of WT and p.Q300* BCAT2 protein expression

Full length cDNA clone of *BCAT2* (Dharmacon) was ligated into the pCMV6-AN-Myc vector (Origene), and the C1121T mutation was introduced by Q5 site directed mutagenesis. Plasmids were transfected into HEK293T cells followed by Western blot analysis as detailed in the **Data Supplement.**

mTOR and P-mTOR (Ser2448) protein expression in mouse hearts

Hearts from *Bcat2* $^{+/+}$ and *Bcat2* $^{pQ330*/pQ330*}$ homozygous males were harvested between 5 and 6 weeks of age and snap frozen in liquid nitrogen. Proteins were extracted from cardiac apex in RIPA buffer and 40 µg of protein was loaded for each sample. Primary antibodies used were mTOR 1:1000 (Cell signalling technology, ref: 2972); mTOR-P-ser2448 1:1000 (Cell signalling technology, ref: 2971), GAPDH 1:10000 (Fitzgerald, ref:10R-G109A), and goat anti-rabbit and anti-mouse horseradish peroxidase–conjugated secondary antibodies from GE Healthcare Life Science (ref: NA9310V and NA9340V, respectively; 1:10000). For each blot, total mTOR and mTOR-P-ser2448 protein expression protein was normalized to the GAPDH signal. Full details are provided in the **Data Supplement**.

Cardiac structural abnormalities

To assess the presence of cardiac hypertrophy, heart weight/body weight and heart weight/tibia length ratios were calculated. Histological assessment of cardiac tissue was carried out on hematoxylin and eosin stained tissue obtained from 6-week-old G3 mice. Both female and male mice were included in the quantification.

ECG measurements, arrhythmia inducibility testing and optical mapping

Surface ECG measurements were performed in mice anesthetized by isoflurane inhalation using the Powerlab acquisition system (ADInstruments). Cardiac arrhythmia inducibility was assessed in isolated, Langendorff-perfused hearts. Atria and ventricles were stimulated at a basic cycle length (BCL) of 120 ms and arrhythmia inducibility was evaluated using up to 3 extrastimuli (S1-S2-S3) and burst pacing. Optical mapping

was carried out in Langendorff-perfused hearts paced at a BCL of 120 ms from the center of the ventricular epicardial surface. Optical action potentials were analyzed, and local activation defined as the maximum positive slope of the action potential was calculated using custom software. Measured local activation times were used to construct ventricular activation maps and calculate conduction velocity in longitudinal and transversal directions. For all electrophysiological measurements, both female and male mice (aged 4-5 weeks) were used. More details can be found in the **Data Supplement**.

Human pluripotent stem cell-derived cardiomyocytes (hPSC-CMs)

Cor4.U control hPSC-CMs were purchased from Ncardia (Leiden, The Netherlands) and were plated on gelatin (0.1% diluted in PBS) coated coverslips at a density of 5000 cells per coverslip following manufacturer's instructions. The generation and use of these cells were conform to the declaration of Helsinki. Cells were first plated in complete culture medium (Ncardia) for 24h and then cultured for 3-4 days in PMC medium (Ncardia) with modified branched chain amino acid (BCAA) concentration. BCAA concentrations in control condition were normalized to 800 nmol/L and supplemented to similar concentrations as quantified by NMR in plasma samples from *Bcat2*$^{p.Q300*/p.Q300*}$ mice (i.e. valine: 10 mmol/L; leucine: 7.5 mmol/L; isoleucine: 4.5 mmol/L). BCAAs were purchased from Sigma-Aldrich and diluted in PMC medium. Rapamycin (Sigma-Aldrich) was dissolved in dimethyl sulfoxide (DMSO) at a stock concentration of 20 mmol/L. For experiments, Rapamycin was used at a concentration of 500 nmol/L diluted in PMC medium (final DMSO concentration 0.0025 %).

Action potential measurements

Details on isolation of ventricular mouse cardiomyocytes and action potential (AP) measurements are provided in the **Data Supplement**. In short, APs were measured at 36 °C and were elicited at 2 Hz in mouse cardiomyocytes and 1 Hz in hPSC-CMs. Typically, hPSC-CMs have a small or even complete lack of the inward rectifying potassium current (I_{K1}). Consequently, hPSC-CMs have a depolarized resting membrane potential (RMP) and are frequently spontaneously active.[18] To overcome these conditions, we injected an *in silico* I_{K1} with kinetics of Kir2.1 channel through dynamic clamp,[19] as previously described and validated.[20,21] Consequently, cells became quiescent with a RMP of around −82 mV. We analysed RMP, AP amplitude (APA), maximal AP upstroke velocity (V_{max}) and APD at 20, 50, and 90% repolarization (APD_{20}, APD_{50}, and APD_{90}, respectively). The fast-pacing protocol used to count and quantify early after depolarizations (EADs), delayed after depolarizations (DADs) and triggered action potentials (TAPs) consisted of 20 pulses at a frequency of 5 Hz followed by a 10 second pause. Average results were obtained from 5 consecutive traces.

Intracellular calcium measurements

Calcium transients were measured at 37^0C in Tyrode solution (see **Data Supplement**) in isolated myocytes stimulated at 6 Hz using the fluorescent probe Indo-1 as described previously.[22] Calcium after-transients were elicited in myocytes stimulated at 6 Hz in which stimulation was stopped and spontaneous activity was recorded for 10 s.[23] Rapid cooling (RC), which causes complete depletion of calcium from the sarcoplasmic reticulum (SR), was used to estimate SR calcium content as described previously.[23] Calcium transient decay time was determined using a mono-exponential fit.

Association between plasma BCAA levels and ECG measures in the KORA F4 Study

The community-based KORA Study (Cooperative Health Research in the Augsburg Region) was conducted in Augsburg, Southern Germany.[14] The KORA F4 Study recruited 3080 participants between 2006 and 2008. All study participants provided written informed consent, and the study was approved by the Bayerische Landesärztekammer and is conform to the declaration of Helsinki. Peripheral blood from fasting individuals was drawn for biomarker analyses. In all participants, a standard 12-lead electrocardiogram (ECG) was obtained after 10 minutes rest in supine position. All participants underwent metabolic profiling using the Biocrates AbsoluteIDQp150 kit (Biocates Life Sciences AG, Innsbruck, Austria). For the current analysis, µmol/l concentrations of the BCAAs valine and xleucine (i.e. the combination of leucine and isoleucine) were used. Further details on data collection and exclusion criteria are provided in the **Data Supplement**. Overall, 776 participants were excluded, leaving 2304 individuals in the final data set.

Statistical analysis

No statistical methods were used to predetermine sample size. Differences between two unpaired groups were assessed using two-tailed *t*-tests when following a normal distribution and Mann-Whitney Rank sum test if normality test failed. Differences comparing 3 groups, when normally distributed were assessed using one-way ANOVA with Student-Newman-Keuls post-hoc test and using one-way ANOVA on ranks (Dunn's method post-hoc) when data were not normally distributed. All statistical tests were performed using sigma stat 3.5 software (Systat Software, Inc). Variability in all plots and graphs is presented as the s.e.m. All $P < 0.05$ were considered to be significant. *$P < 0.05$; **$P \leq 0.01$; #$P \leq 0.001$. Summary statistics are depicted in **Supplemental Tables S2-9**. To determine a relation between ECG measures and BCAAs in the KORA population, linear regression models were fitted, adjusting for sex. Multiplicative interaction terms showed no statistical interactions with age or sex, and interaction terms were removed from the final models. All statistical analyses in KORA were performed using STATA 12.0 (StataCorp LP, College Station, TX, USA).

RESULTS

Sudden death phenotype in homozygous *Bcat2*^{C1121T} mice

Following ENU mutagenesis of C57BL/6J male mice (G_0) and successive rounds of breeding with C3H.Pde6b+ females (**Fig. 1A**), G3 cohorts of mutagenized animals were produced for longitudinal phenotyping studies as part of the Harwell Ageing Screen.[11] Mice from a single pedigree, consisting of mixed background G3 mice died suddenly with no obvious cause and in the absence of preceding symptoms such as tremoring or gait abnormalities, between 6 and 9 weeks of age (batch A; **Fig. 1B**). Mapping was performed on the basis that homozygous ENU induced mutations must lay in a region of C57BL/6J homogeneity and a region was identified on chromosome 7 spanning from 28.8Mb to 56.1Mb. Whole genome sequencing of the G1 founder male revealed two high confidence coding mutations within the mapped region, *Bcat2*^{C1121T} and *Siglech*^{C751T} resulting in a Q300* and Q219* nonsense mutation, respectively. Pyrosequencing confirmed that both mutations were present in individuals affected by the sudden death phenotype but absent from unaffected controls. Further breeding eliminated *Siglech* as a candidate by narrowing the mapped region and confirmed that all affected mice suffering sudden death were homozygous for the nonsense mutation *Bcat2*^{C1121T} in the gene encoding branched chain aminotransferase 2 **(Suppl. Fig. S1)**. No heterozygous *Bcat2*^{C1121T} or wild-type mice succumbed to sudden death before the age of eight weeks and no homozygous mice lived beyond this age (batch B; **Fig. 2A**). The *Bcat2*^{C1121T} mutation results in an early stop (Q300*) and consequently a truncated BCAT2 protein lacking the CXXC motif essential for enzyme catalytic activity and substrate orientation (**Suppl. Fig. S2)**. Plasma clinical chemistry revealed increased levels of triglycerides, fatty acids, and glycerol, as well as LDL in homozygous *Bcat2*$^{p.Q300*/p.Q300*}$ mice and intermediate levels in heterozygous *Bcat2*$^{+/p.Q300*}$ mice (**Suppl. Fig. S3 and Suppl. Table S3**). Homozygous *Bcat2*$^{p.Q300*/p.Q300*}$ mice exhibited increased potassium but decreased chloride concentration in plasma, and increased iron levels. Whilst significant, none of these data provide a clear explanation for the sudden death phenotype.

Accumulation of branched chain amino acids in plasma and urine of *Bcat2*$^{p.Q300*/p.Q300*}$

BCAT2 is located in the mitochondria of most cells of the body, and is responsible for catabolizing BCAAs (leucine, isoleucine, and valine), essential amino acids that must be obtained from dietary sources. Following catabolism to their respective α-keto acids (BCKA), BCAAs are further catabolized by the branched-chain keto acid dehydrogenase complex (BCKDC), and the final catabolic products (acetyl-CoA and succinyl-CoA) are ultimately consumed in mitochondria for respiration through the tri-carboxylic acid cycle.[24] In line with this, NMR analysis of plasma revealed an up to 10-fold increase in plasma levels of BCAAs (but no increase in BCKAs, which were under the detection threshold) in *Bcat2*$^{p.Q300*/p.Q300*}$ mice aged 5 weeks (**Fig. 2B-D**). Similar accumulation of BCAAs was observed in the urine of mutant mice aged 5 weeks (**Suppl. Fig. S4**). Hence, the identified mutation resulted in a truncated BCAT protein with consequent

accumulation of BCAAs but not BCKAs. Heterozygous *Bcat2*$^{+/p.Q300*}$ mice did not display sudden death or any other overt phenotype up to the age of 6-8 months, showed normal BCAA plasma levels (**Fig. 2B-D**), and hence were not investigated further.

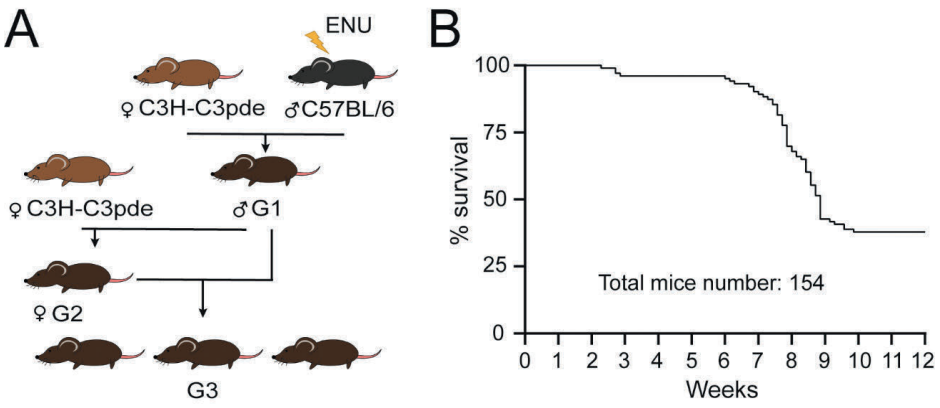

Figure 1. ENU mutagenesis induced sudden death phenotype in young mice. A, *Breeding scheme used to produce G3 phenotyping cohorts. C57BL/6J males were mutagenized with ENU and crossed to C3H.Pde6b+ females. G1 males were then crossed again to C3H.Pde6b+ females, producing a G2 generation. Finally, G2 females were crossed to the G1 male parent to produce a G3 phenotyping cohort.* **B**, *Mortality curve of the initial G3 phenotyping pedigrees (batch A; n=154 mice) demonstrating a clear early death phenotype between 6 and 9 weeks of age.*

Bcat2$^{p.Q300*/p.Q300*}$ mice display cardiac electrical alterations and increased arrhythmia inducibility

Given the absence of overt prior symptoms in *Bcat2*$^{p.Q300*/p.Q300*}$ mice, we hypothesized a cardiac basis for their sudden death. No cardiac structural changes such as hypertrophy, dilation or fibrosis were observed in *Bcat2*$^{p.Q300*/p.Q300*}$ hearts upon histological examination (**Suppl. Fig. S5A-C, Suppl. Table 2**). We therefore performed detailed electrophysiological analysis in mice aged 4-5 weeks, well before the age of 6 weeks at which they started dying suddenly. Due to their young age and hence small size, and considering needed recovery time post-surgery, *in vivo* telemetric Holter monitoring was not possible. However, surface electrocardiograms (ECGs) under isoflurane anaesthesia revealed significantly prolonged QT, QTc and PR intervals in *Bcat2*$^{p.Q300*/p.Q300*}$ compared to *Bcat2*$^{+/+}$ mice (**Fig. 3A-B, Suppl. Table S2**). We next investigated the *ex vivo* cardiac electrophysiological differences between *Bcat2*$^{+/+}$ and *Bcat2*$^{p.Q300*/p.Q300*}$ isolated, Langendorff-perfused hearts. Atrio-ventricular (AV) conduction time was significantly increased in *Bcat2*$^{p.Q300*/p.Q300*}$ mice (**Fig. 3C-D, Suppl. Table S2)**, similar to the increased PR-interval observed on ECG analysis. Optical mapping experiments revealed no differences in ventricular conduction between the groups (**Suppl. Fig. S6A-B, Suppl. Table S2**). Nevertheless, repolarization time (APD_{70}) was significantly

prolonged in *Bcat2*$^{p.Q300*/p.Q300*}$ compared to *Bcat2*$^{+/+}$ hearts (60.4 ± 6.0 ms and 43.9 ± 3.1, respectively; $p<0.05$ – **Fig. 3E-F**), in line with the observed QTc-prolongation on the surface ECG. Furthermore, the difference between the longest and shortest APD70 was also significantly increased in *Bcat2*$^{p.Q300*/p.Q300*}$ (16.3 ± 1.3 ms) as compared to *Bcat2*$^{+/+}$ hearts (9.1 ± 1.3 ms; $p<0.05$) (**Suppl. Table S2**), suggesting increased pro-arrhythmic APD heterogeneity. Arrhythmia inducibility studies in Langendorff-perfused hearts showed an increased incidence of inducible arrhythmias in *Bcat2*$^{p.Q300*/p.Q300*}$ mice compared to *Bcat2*$^{+/+}$ (50% versus 11.1% respectively, the majority of which were non-sustained (**Fig. 3G-H**).

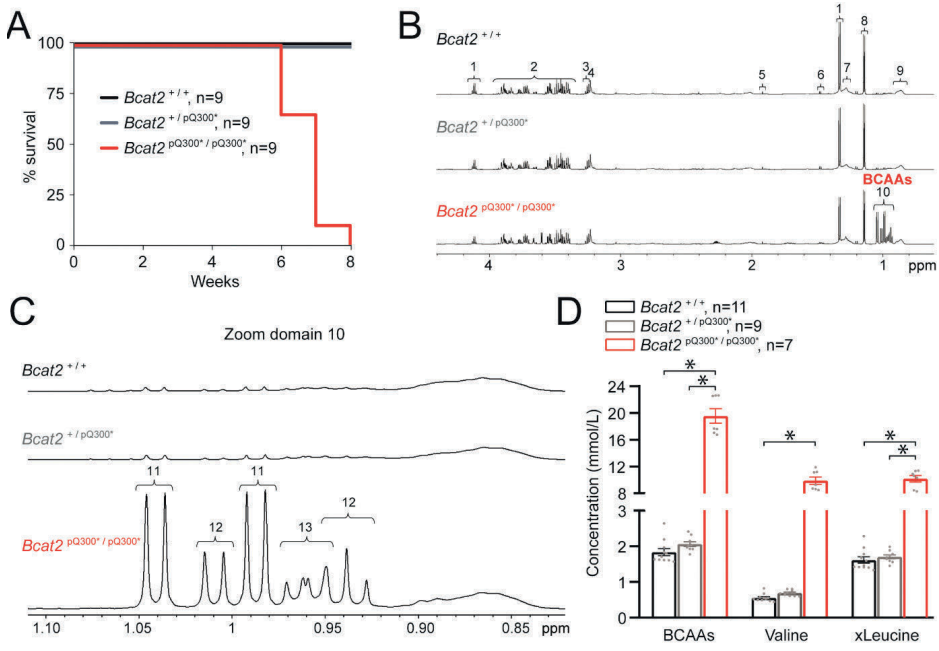

Figure 2: Homozygous *Bcat2*$^{p.Q300*/p.Q300*}$ mice display sudden death and increased plasma BCAA levels at young age. A, *Mortality curve displaying death of all homozygous Bcat2*$^{p.Q300*/p.Q300*}$ *mice (batch B) by the age of 8 weeks.* **B**, *Illustrative water suppressed spin-echo proton NMR spectra of free-fed plasma from Bcat2*$^{+/+}$, *Bcat2*$^{+/p.Q300*}$, *and Bcat2*$^{p.Q300*/p.Q300*}$ *mice at 5 weeks of age. The NMR spectra were plotted such that the αC1 proton of glucose at 5.23ppm (not shown) was of similar intensity in each data set. The prominent metabolites shown in the expanded region are assigned to: 1) lactate, 2) glucose, 3) including β-glucose, 4) choline-containing compounds, 5) acetate, 6) alanine, 7) mobile lipid* CH_2, *8) 2,3-butanediol, 9) mobile lipid* CH_3, *10) branched chain amino acids (BCAAs).* **C**, *NMR spectra from Bcat2*$^{+/+}$, *Bcat2*$^{+/p.Q300*}$, *Bcat2*$^{p.Q300*/p.Q300*}$ *further expanded (zoom domain 10) to illustrate the branched chain amino acid -*CH_3 *region with metabolites assigned to 11) valine, 12) isoleucine, 13) leucine.* **D**, *BCAA plasmatic quantification in Bcat2*$^{+/+}$ *(n=11), Bcat2*$^{+/p.Q300*}$ *(n=9) and Bcat2*$^{p.Q300*/p.Q300*}$ *(n=7) mice. *p<0.05, one-way ANOVA on ranks with post-hoc Dunn's method.*

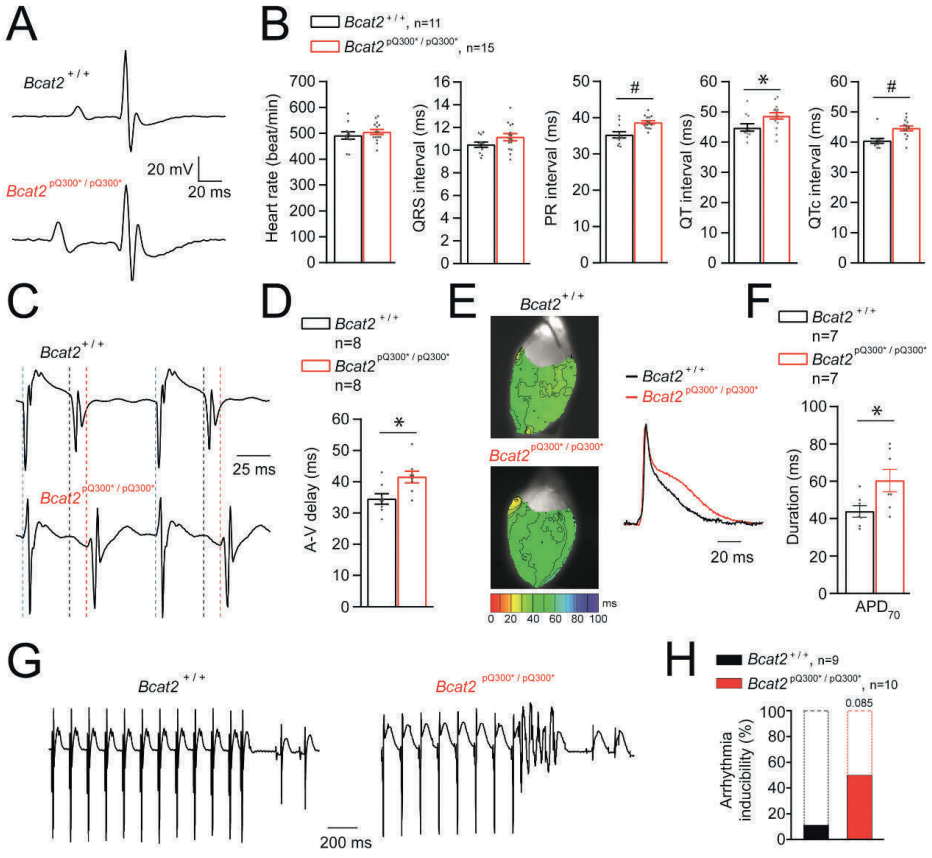

Figure 3: Homozygous *Bcat2*$^{p.Q300*/p.Q300*}$ mice display ECG abnormalities *in vivo* and atrio-ventricular delay, prolonged repolarization and arrhythmia inducibility *ex vivo*. A, *Typical ECG traces obtained under isoflurane anaesthesia for Bcat2$^{+/+}$ and Bcat2$^{p.Q300*/p.Q300*}$ mice.* **B,** *Average values for heart rate, QRS interval, PR interval, QT and QTc (corrected) for both Bcat2$^{+/+}$ (n=11) and Bcat2$^{p.Q300*/p.Q300*}$ (n=15) mice aged 4-5 weeks.* **C**, *Typical examples of atrio-ventricular (AV) delay measurements in Langendorff-perfused isolated hearts (right atrial stimulation at a basic cycle length of 120 ms).* **D**, *Average values for AV-delay in Bcat2$^{+/+}$ and Bcat2$^{p.Q300*/p.Q300*}$ hearts.* **E**, *Typical left ventricular repolarization maps obtained from optical mapping experiments on perfused explanted hearts during central stimulation (6.6 Hz).* **F**, *Average APD_{70} (action potential duration at 70% of repolarization) values for Bcat2$^{+/+}$ (n=7) and Bcat2$^{p.Q300*/p.Q300*}$ (n=7) mice. *p<0.05, Student's t-test.* **G**, *Typical example of a short run of ventricular tachycardia induced in an isolated, Langendorff-perfused Bcat2$^{p.Q300*/p.Q300*}$ heart following a short-coupled paced beat.* **H**, *Bar graph representing the percentage of arrhythmic events recorded on Bcat2$^{+/+}$ and Bcat$^{p.Q300*/p.Q300*}$ mouse explanted hearts. *p<0.05, Student's t-test.*

Action potential prolongation, calcium dysregulation, and pro-arrhythmic events in *Bcat2*$^{p.Q300*/p.Q300*}$ cardiomyocytes

We next investigated the cellular electrophysiological alterations underlying the observed pro-arrhythmia in *Bcat2*$^{p.Q300*/p.Q300*}$ mice. **Fig. 4A** shows typical action potentials (APs) and maximal upstroke velocities (V_{max}) elicited at a pacing frequency of 2 Hz in isolated left ventricular cardiomyocytes isolated from *Bcat2*$^{+/+}$ and *Bcat2*$^{p.Q300*/p.Q300*}$ hearts. V_{max}, AP amplitude (APA), and AP duration at 90% repolarization (APD_{90}) were significantly increased in *Bcat2*$^{p.Q300*/p.Q300*}$ compared to *Bcat2*$^{+/+}$ cardiomyocytes (**Fig. 4B, Suppl. Table S4**). Using a fast pacing (20 pulses at 5 Hz) protocol, the presence of pro-arrhythmic events was evaluated, including early after depolarizations (EADs), delayed after depolarizations (DADs) and triggered action potentials (TAPs) (indicated by arrows in **Fig. 4C**). The incidence of TAPs and EADs was significantly higher in *Bcat2*$^{p.Q300*/p.Q300*}$ as compared to *Bcat2*$^{+/+}$ cardiomyocytes (**Fig. 4D**). The observed increase in $V_{max,}$ APD_{90} and EAD incidence was not associated with alterations in sodium current: although *Bcat2*$^{p.Q300*/p.Q300*}$ cardiomyocytes showed a hyperpolarizing shift in both activation and inactivation, the peak current density, window current, and late sodium current density were not altered (**Suppl. Fig. S7, Suppl. Table S4**).

Since intracellular calcium dysregulation often underlies pro-arrhythmic DADs and TAPs, we next explored calcium homeostasis in isolated cardiomyocytes. **Fig. 5A** shows typical calcium concentration ($[Ca^{2+}]_i$) transients elicited at a pacing frequency of 6 Hz. On average, *Bcat2*$^{p.Q300*/p.Q300*}$ cardiomyocytes showed increased intracellular diastolic calcium levels ($[Ca^{2+}]_i$), higher $[Ca^{2+}]_i$ transients, and increased transient amplitudes as compared to *Bcat2*$^{+/+}$ cells (**Fig. 5B, Suppl. Table S5**). Sarcoplasmic reticulum (SR) content measured by rapid cooling was also significantly increased in *Bcat2*$^{p.Q300*/p.Q300*}$ cardiomyocytes (**Suppl. Fig. S8A-B**), while the ratio between diastolic $[Ca^{2+}]_i$ and SR content was not different between groups (**Suppl. Table S5**). Moreover, mRNA expression levels of *Slc8a1* (NCX) and *Atp2a2* (SERCA) were unchanged (**Suppl. Fig. S9, Suppl. Table S2**). **Fig. 5C** shows typical examples of calcium after-transients recorded following a fast-pacing protocol (20 pulses at 6 Hz) using field stimulation. These calcium after-transients were separated into two groups based on their amplitude: 1) after-transients of low amplitude considered not to trigger an AP, and 2) high-amplitude after-transients capable of triggering an AP (i.e. TAP). The total number of calcium after-transients (triggered and non-triggered combined) was significantly higher in *Bcat2*$^{p.Q300*/p.Q300*}$ compared to *Bcat2*$^{+/+}$ cardiomyocytes (**Fig. 5C-D, Suppl. Table S5**), indicating a calcium-dependent pro-arrhythmia mechanism. The addition of 50 nmol/l noradrenaline significantly increased diastolic $[Ca^{2+}]_i$, systolic $[Ca^{2+}]_i$ and transient amplitude in *Bcat2*$^{+/+}$ cardiomyocytes, but only marginally in *Bcat2*$^{p.Q300*/p.Q300*}$ cardiomyocytes (**Suppl. Table S5**). Nevertheless, noradrenaline significantly increased the number of calcium after-transients in both *Bcat2*$^{+/+}$ and *Bcat2*$^{p.Q300*/p.Q300*}$ cardiomyocytes (**Suppl. Table S5**).

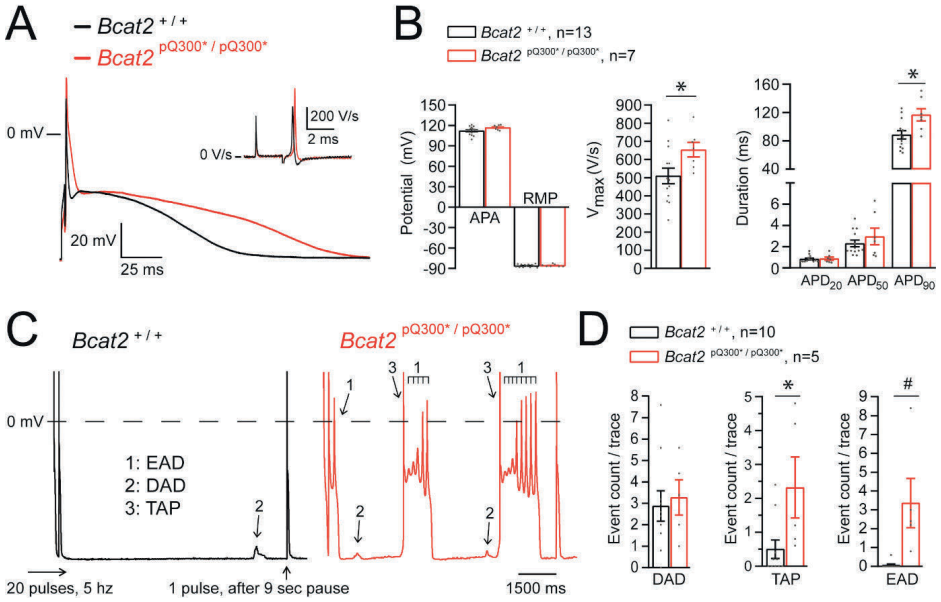

Figure 4: Abnormal repolarization and pro-arrhythmic events in *Bcat*$^{p.Q300*/p.Q300*}$ isolated cardiomyocytes. A, *Typical examples of action potentials (AP) and upstroke velocities (dV/dt$_{max}$; inset) elicited at a stimulation frequency of 2 Hz in left ventricular (LV) isolated cardiomyocytes from Bcat2$^{+/+}$ and Bcat2$^{p.Q300*/p.Q300*}$ mice aged 4-5 weeks.* **B**, *Average values for APA (action potential amplitude), RMP (resting membrane potential), V$_{max}$ (upstroke velocity) and APD (action potential duration) at 20%, 50% and 90% repolarization (APD$_{20}$, APD$_{50}$, APD$_{90}$) of LV cardiomyocytes isolated from Bcat2$^{+/+}$ (n=15 cells from 6 independent cardiomyocyte dissociations) and Bcat2$^{p.Q300*/p.Q300*}$ (n=9 cells from 5 independent cardiomyocyte dissociations) mice.* **C**, *Typical examples of early afterdepolarizations (EADs: 1), delayed afterdepolarizations (DADs: 2) and triggered action potentials (TAPs: 3) recorded after a fast pacing stimulation protocol (20 pulses at 5 Hz followed by a 9s pause and 1 pulse followed by a 500ms pause) in Bcat2$^{+/+}$ and Bcat2$^{p.Q300*/p.Q300*}$ LV cardiomyocytes.* **D**, *Average count per trace for DADs, TAPs and EADs observed in Bcat2$^{+/+}$ (n = 10 cardiomyocytes from 6 mice) and Bcat2$^{p.Q300*/p.Q300*}$ mice (n = 5 cardiomyocytes from 4 mice). Average numbers were calculated using five consecutive traces. (with Student's t-test or Mann-Whitney Rank sum test)***.**

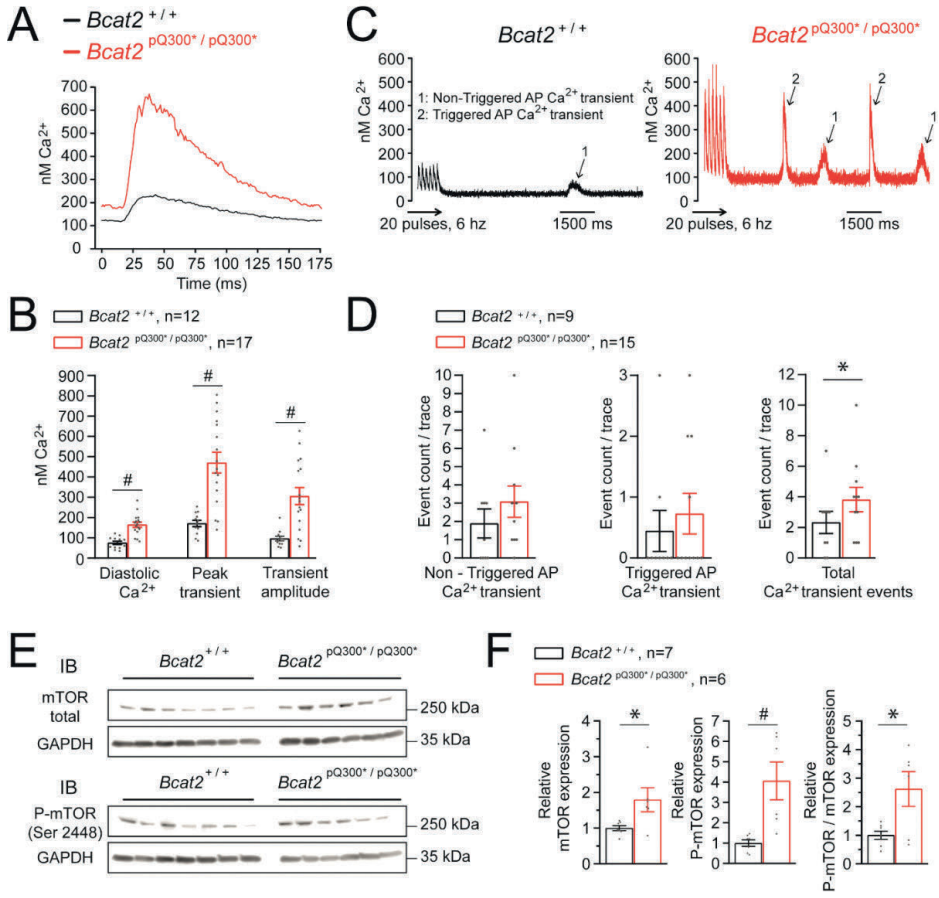

Figure 5: Abnormal intracellular calcium and myocardial mTOR upregulation in *Bcat2*$^{p.Q300*/p.Q300*}$ mice. A, *Typical intracellular calcium transient recording performed at a pacing frequency of 6 Hz and* **B**, *average values for diastolic Ca^{2+}, peak transient and transient amplitude of LV cardiomyocytes from Bcat2$^{+/+}$ (n=12 cardiomyocytes from 5 independent cardiomyocyte dissociations) and Bcat2$^{p.Q300*/p.Q300*}$ (n=17 cardiomyocytes from 4 independent cardiomyocyte dissociations) mice aged 4-5 weeks.* **C**, *Typical example of calcium after-transients in isolated cardiomyocytes from Bcat2$^{+/+}$ and Bcat2$^{p.Q300*/p.Q300*}$ cardiomyocytes following a fast pacing protocol using field stimulation and* **D**, *quantification of non-triggered action potential (AP) Ca^{2+} transient, triggered AP Ca^{2+} transient and total Ca^{2+} transient events in Bcat2$^{+/+}$ (n = 9 cardiomyocytes from 3 mice) and Bcat2$^{p.Q300*/p.Q300*}$ mice (n = 15 cardiomyocytes from 4 mice).* **E**, *Representative immunoblots of total mTOR, phosphorylated mTOR (P-mTOR) at ser2448 and GAPDH from heart lysates (apex) from Bcat2$^{+/+}$ and Bcat2$^{p.Q300*/p.Q300*}$ mice.* **F**, *average total mTOR and phosphorylated P-mTOR expression normalized to GAPDH, and ratio of normalized P-mTOR on normalized total mTOR from Bcat2$^{+/+}$ (n=7) and Bcat2$^{p.Q300*/p.Q300*}$ (n=6) mouse heart lysates.*P<0.05; #P≤0.001 (with Student's t-test or Mann-Whitney Rank sum test).*

Direct pro-arrhythmic effects of BCAAs in human PSC-derived cardiomyocytes

To demonstrate a direct causal link between elevated BCAAs and pro-arrhythmia, we evaluated the cellular electrophysiological consequences of increased BCAA levels in cultured human PSC-derived cardiomyocytes (hPSC-CMs). Incubation of hPSC-CMs for 5 days with BCAA levels similar to those observed in plasma of *Bcat2*$^{p.Q300*/p.Q300*}$ mice resulted in significant prolongation of APD_{90} (**Fig. 6A-B, Suppl. Table S6**), and significantly increased the occurrence of pro-arrhythmic early and delayed afterdepolarizations (EAD/DAD) as compared to hPSC-CMs cultured in control medium (**Fig. 6C-D, Suppl. Table S6**), hence recapitulating the findings observed in *Bcat2*$^{p.Q300*/p.Q300*}$ cardiomyocytes. Incubation of valine alone induced similar APD_{90} prolongation and increased EAD/DAD incidence, while alanine (as a general amino acid control) had no effects (**Suppl. Fig. S10A-D, Suppl. Table S8**). Similar to *Bcat2*$^{p.Q300*/p.Q300*}$ cardiomyocytes, hPSC-CMs cultured in medium with increased BCAA concentration also displayed intracellular calcium dysregulation, including increased diastolic $[Ca^{2+}]_i$ and after-transients (**Fig. 7A-D, Suppl. Table S6**), further confirming a direct pro-arrhythmic effect.

Pro-arrhythmic effects of elevated BCAA levels are mediated by mTOR pathway activation

In addition to their role in energy balance, BCAAs function as potent nutrient signal molecules to promote protein synthesis, cellular metabolism, and cell growth in a mammalian target of rapamycin (mTOR)-dependent manner,[24,25] and elevated BCAA concentrations have been shown to lead to chronic induction of mTOR activity and increased oxidative stress.[26,27] Indeed, cardiac tissue from *Bcat2*$^{p.Q300*/p.Q300*}$ mice showed significantly higher expression levels of both mTOR total protein and activated P-mTOR as compared to *Bcat2*$^{+/+}$ (normalized for GAPDH), in addition to an increased P-mTOR to mTOR ratio, indicating mTOR pathway activation (**Fig. 5E-F, Suppl. Table S2**). In line with mTOR pathway activation, the mRNA expression level of the pro-hypertrophic marker *Anf* was also significantly increased in *Bcat2*$^{p.Q300*/p.Q300*}$ hearts (**Suppl. Fig. S9, Suppl. Table S2**). The functional contribution of mTOR pathway activation to the observed pro-arrhythmic effects of BCAAs was subsequently demonstrated in hPSC-CMs. Incubation with the mTOR inhibitor rapamycin (500 nmol/L) prevented the APD_{90} prolongation and EAD/DAD incidence (**Fig. 6A-D**), as well as the calcium dysregulation and after-transient occurrence (**Fig. 7A-D**) induced by increased BCAA levels (**Suppl. Table S6**), whereas it had no electrophysiological effects in the absence of high BCAA levels (**Suppl. Table S7**). These observations demonstrate the functional involvement of mTOR pathway activation in the pro-arrhythmic effects of elevated BCAA levels.

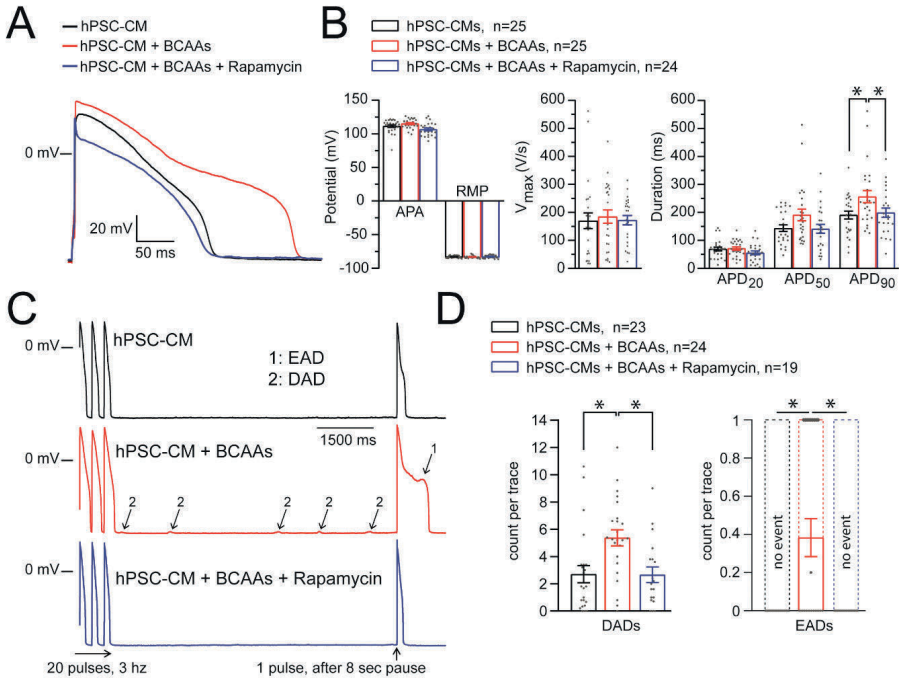

Figure 6: Increased levels of BCAAs recapitulate the pro-arrhythmic phenotype in hPSC derived cardiomyocytes (hPSC-CMs) which is reversible upon mTOR inhibition. A, *Typical example of APs elicited at a stimulation frequency of 1 Hz from hPSC-CMs incubated with control medium or with increased levels of BCAAs in the presence or absence of the mTOR inhibitor rapamycin (500 nmol/L).* **B**, *Average values for APA (AP amplitude), RMP (resting membrane potential), V_{max} (up-stroke velocity) and APD (action potential duration) at 20%, 50% and 90% repolarization (APD_{20}, APD_{50}, APD_{90}) of hPSC-CMs incubated with the control medium (n=25 hPSC-CMs from 5 dissociations), with increased levels of BCAAs (n=25 hPSC-CMs from 5 dissociations), and with increased BCAA levels and rapamycin (n=24 hPSC-CMs from 5 dissociations).* **C**, *Typical examples of EADs (1) and DADs (2) recorded after a fast-pacing stimulation protocol (20 pulses at 3 Hz followed by an 8s pause and 1 pulse followed by a 1s pause).* **D**, *Average count per trace for DADs and EADs observed in hPSC-CMs incubated with the control medium (n=23 hPSC-CMs from 5 dissociations), with increased levels of BCAAs (n=24 hPSC-CMs from 5 dissociations), and with increased BCAA levels and rapamycin (n=19 hPSC-CMs from 5 dissociations). Average numbers were calculated using five consecutive traces. *P<0.05, one-way ANOVA (with Student-Newman-Keuls Method post-hoc test) or one-way ANOVA on ranks (with Dunn's method post-hoc test).*

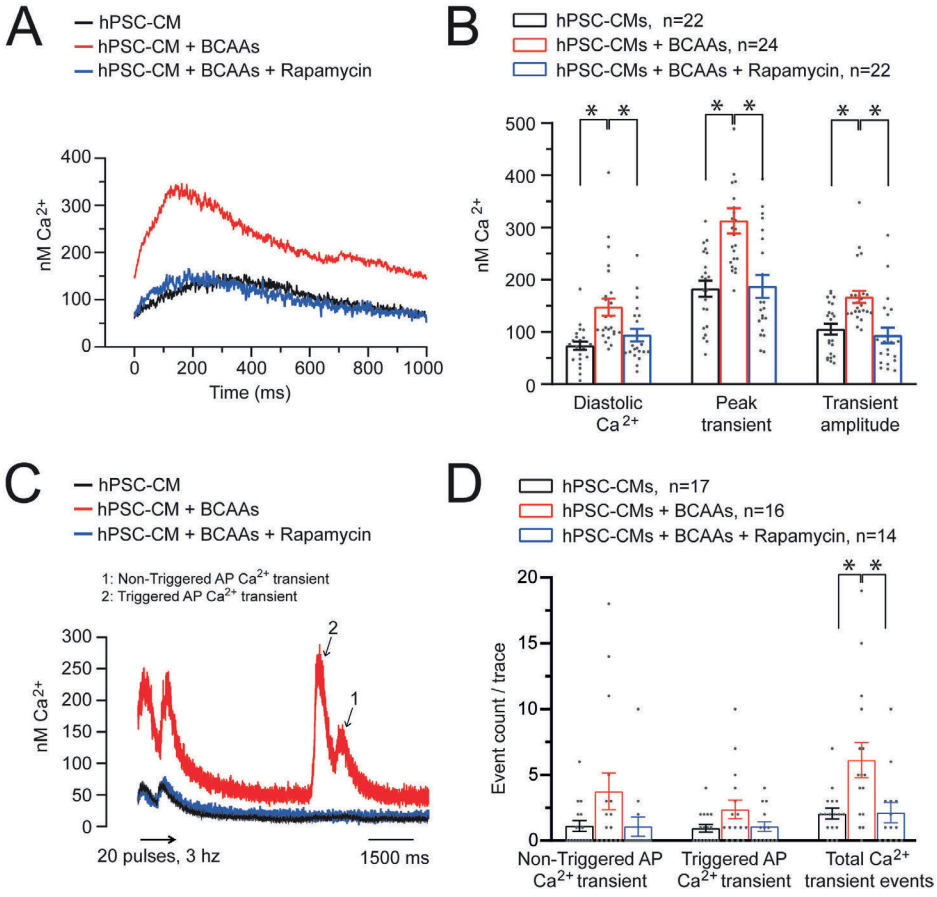

Figure 7: Abnormal intracellular calcium regulation in human PSC derived cardiomyocytes (hPSC-CMs) with elevated BCAAs is reversible upon mTOR inhibition. A, *Typical examples of intracellular calcium transient recordings in hPSC-CMs performed at a pacing frequency of 1 Hz.* **B**, *Average values for diastolic Ca^{2+}, peak transient and transient amplitude with control medium (n=22 hPSC-CMs from 3 dissociations), increased BCAA levels (n=24 hPSC-CMs from 3 dissociations), and with increased BCAA levels and rapamycin at 500 nmol.L^{-1} (n=22 hPSC-CMs from 3 dissociations).* **C**, *Typical example of calcium after-transients in hPSC-CMs incubated with a control medium or with increased levels of BCAAs following a fast-pacing protocol using field stimulation and* **D**, *quantification of non-triggered action potential (AP) Ca^{2+} transient, triggered AP Ca^{2+} transient and total Ca^{2+} transient events in hPSC-CMs incubated with the control medium (n=17 hPSC-CMs from 2 dissociations), with increased levels of BCAAs (n=16 hPSC-CMs from 2 dissociations), and with increased BCAA levels and rapamycin (n=14 hPSC-CMs from 2 dissociations). *P<0.05, one-way ANOVA on ranks (with Dunn's method post-hoc test).*

Plasma BCAA levels correlate with ECG parameters in the general population

Finally, to confirm a modulatory role of BCAAs on cardiac electrical function in humans, we investigated the relation between ECG measures and BCAA plasma levels in 2304 participants (mean age 51.5±10.6 years; 52.6% women) from the German community-based KORA F4 Study.[14] Average ECG parameters were: heart rate 63.8±9.7 bpm, PR interval 165.9±23.2 ms, QRS duration 93.4±11.8 ms, QTc interval 422.3±20.4 ms. The mean concentration of valine was 275.4±60.2 µmol/l and of xleucine was 213.2±45.2 µmol/l. Both valine and xLeucine followed a normal distribution, and showed a linear relation with ECG parameters (**Suppl. Fig. S11**). Regression results between ECG measures and BCAAs are presented in **Table 1**. We observed significant sex-adjusted associations between fasting valine plasma levels and the ECG parameters PR interval, QRS duration, and QTc interval. This association was consistent across men and women for the PR interval, and maintained effect directionality for QRS duration and QTc interval. Overall, the effect size was strongest for PR interval (beta: 0.0335±0.0085 ms/µmol/l; $p<0.001$), for which we also identified a significant association with xLeucine (i.e. the combination of Leucine and Isoleucine; beta: 0.0270±0.0125 ms/µmol/l; $p<0.05$). Together with the observations in *Bcat2*$^{p.Q300*/p.Q300*}$ mice, these findings indicate that higher plasma BCAA levels are associated with altered cardiac conduction and repolarization.

Table 1. Association of ECG measures with branched-chain amino acids in the KORA F4 Study.

		Unstratified		Men		Women	
ECG measure	**BCAA**	**Beta (SE)**	**P**	**Beta (SE)**	**P**	**Beta (SE)**	**P**
Heart rate [bpm]	Valine [µmol/L]	0.0035 (0.0036)	0.34	0.0017 (0.0053)	0.75	0.0054 (0.0050)	0.28
	xLeucine [µmol/L]	0.0026 (0.0053)	0.61	0.0051 (0.0073)	0.49	-0.0004 (0.0077)	0.96
PR [ms]	Valine [µmol/L]	0.0335 (0.0085)	**<0.001**	0.0264 (0.0126)	**0.036**	0.0410 (0.0115)	**<0.001**
	xLeucine [µmol/L]	0.0270 (0.0125)	**0.031**	0.0226 (0.0175)	0.20	0.0327 (0.0179)	0.07
QRS [ms]	Valine [µmol/L]	-0.0086 (0.0042)	**0.040**	-0.0134 (0.0062)	**0.030**	-0.0034 (0.0056)	0.54
	xLeucine [µmol/L]	-0.0069 (0.0061)	0.26	-0.0134 (0.0086)	0.12	0.0016 (0.0087)	0.86
QTc [ms]	Valine [µmol/L]	0.0234 (0.0075)	**0.002**	0.0173 (0.0108)	0.11	0.0297 (0.0104)	**0.004**
	xLeucine [µmol/L]	0.0144 (0.0110)	0.19	0.0032 (0.0150)	0.83	0.0287 (0.0161)	0.08

Linear regression models excluded participants ≤50 kg body weight, ≥70 years of age, or with diabetes mellitus. Unstratified models adjusted for sex. Beta: Standardized regression coefficient. SE: Standard error. P: p value.

DISCUSSION

Through a phenotype-driven random mutagenesis screen[11] we here identified a mutant mouse line presenting with a striking, highly penetrant phenotype of sudden death without prior symptoms. The causative mutation was determined to be a nonsense mutation in the *Bcat2* gene resulting in a defect in BCAA catabolism and the accumulation of high levels of BCAAs in plasma and urine. Detailed electrophysiological studies unravelled a robust arrhythmogenic phenotype in affected mice, and additional studies in hPSC-CMs confirmed a direct pro-arrhythmic effect of elevated BCAAs levels. We therefore identified for the first time a role for BCAA dysregulation in modulating cardiac electrophysiology and risk for cardiac arrhythmias and sudden death.

BCAT2 is located in the mitochondria of most cells of the body, and is responsible for catabolizing branched chain amino acids (BCAAs; leucine, isoleucine, and valine), essential amino acids that must be obtained from dietary sources. Following catabolism by either BCAT2 or BCAT1 (the cytosolic isoform) to their respective α-keto acids (BCKA), BCAAs are further catabolized by the branched-chain keto acid dehydrogenase complex (BCKDC).[24] The final catabolic products of BCAAs are consumed in mitochondria for respiration through the tri-carboxylic acid cycle. Defects in BCAA catabolism have been associated with the development of Maple Syrup Urine disease (MSUD), an autosomal recessive metabolic disorder associated with brain damage caused by mutations in genes of the branched chain BCKDC complex.[24] Here, the block in BCAA catabolism prevents the catabolism of BCKAs, the catabolic product resulting from the action of the two BCAT enzymes, cytosolic and mitochondrial. MSUD patients exhibit a failure to thrive and neurological deterioration thought to be associated with the accumulation of BCKAs.[24] This was mirrored in a different, previously published mouse line with an ENU-induced *Bcat2*, which resulted in the 5' splice site in *Bcat2* and the deletion of exon 2 with an absence of mature BCAT2 protein.[28] These mutant mice displayed failure to thrive, reduced body weight and early death; no details were provided on the early death phenotype, and cardiac (electrophysiological) characterisation was not performed. Analysis of the plasma revealed increased levels of both BCAAs (albeit it to a lower extent as compared to *Bcat2*$^{p.Q300*/p.Q300*}$ mice) and BCKAs, with the latter prevented from entering the mitochondria and therefore accumulating. In contrast, our *Bcat2*$^{p.Q300*/p.Q300*}$ mutation results in the production of a truncated protein, no differences in body weight, an accumulation of BCAAs but not BCKAs, and a sudden death phenotype. In particular, the absence of neuronal damage is likely due to the fact that BCKAs in *Bcat2*$^{p.Q300*/p.Q300*}$ mice were not elevated and hence glutamate signalling not disturbed. Mice with targeted deletion of exon 4-6 of *Bcat2* demonstrated lower body weight and exercise intolerance, while their BCKA plasma levels remained normal.[29] The lack of accumulation of BCKAs in our mice implies that the BCKA transport mechanism is intact in *Bcat2*$^{p.Q300*/p.Q300*}$ mice but not in the previously described *Bcat2* deficient mice, as catabolism of BCKAs occurs within the mitochondria.[24] This suggests that the truncated

BCAT2^{Q300*} protein has impaired transamination activity yet retained BCKA transport activity[30,31] either in the truncated protein or by maintaining the interaction of BCAT2 with a separate transport protein. This is supported by the observation that in our mice the concentration of valine is higher than that observed in the null mice. Hence, our novel mouse model presenting specific BCAA accumulation in the absence of BCKAs allows the investigation of the physiological effects of an excess of BCAAs, and the dissection of the transamination and BCKA transport activities of BCAT2. Additionally, all murine *Bcat2* models described so far were generated in C57BL/6J mice, a murine strain known to present distinct mitochondrial calcium and reactive oxygen species handling properties demonstrated to be protective in heart failure models.[32] In our present study, after the initial ENU mutagenesis step, mice were backcrossed onto the C3H background strain which may explain the severe phenotype severity observed in *Bcat2*$^{p.Q300*/p.Q300*}$ mice.

Our findings identify a profound effect of elevated BCAA levels on intracellular calcium handling. Despite the substantial increase in diastolic and systolic $[Ca^{2+}]_i$ in *Bcat2*$^{p.Q300*/p.Q300*}$ cardiomyocytes, the Ca^{2+} gradient across the SR membrane and the decay time of the Ca^{2+} transient remained unaltered, arguing against underlying alterations in phosphorylation state. Taken together, we consider the altered diastolic $[Ca^{2+}]_i$ as the main driver for the observed pro-arrhythmic calcium dysregulation in *Bcat2*$^{p.Q300*/p.Q300*}$ cardiomyocytes. Elevated diastolic Ca^{2+}, which has been shown to increase both the systolic Ca^{2+} as well as the SR Ca^{2+} content,[33] may be the consequence of various processes affecting ionic gradients across cell membranes, including altered energetic metabolism. Together with the increase in SR Ca^{2+}, elevated diastolic Ca^{2+} leads to a higher open probability of the ryanodine channels and the likelihood of spontaneous Ca^{2+} release from the SR. Subsequent calcium removal by the sodium/calcium exchanger (NCX) may then lead to membrane (after)depolarization and onset of arrhythmia. Of note, late sodium current density was not altered and hence unlikely to have contributed to the AP prolongation, EAD incidence and Ca^{2+} dysregulation observed in in *Bcat2*$^{p.Q300*/p.Q300*}$ cardiomyocytes. In line with the *in vivo* and *ex vivo* findings in the *Bcat2*$^{p.Q300*/p.Q300*}$ mice, atrio-ventricular conduction (PR interval) and repolarization (QT interval) ECG traits were significantly correlated with BCAA plasma concentrations in the KORA cohort. These results indicate a modulatory effect of BCAAs on electrophysiological characteristics of both the working myocardium and the cardiac conduction system, suggesting that ventricular arrhythmias as well as conduction defects could be triggered by elevated BCAA levels. Conduction through the central part of the AV-node is mainly calcium-driven, and we have recently demonstrated that intracellular calcium dysregulation may significantly contribute to AV-conduction.[34] Hence, BCAA-induced calcium dysregulation may affect AV-conduction through prolonged repolarization and/or reduced gap junctional conductance within the central AV-node. Additionally, while myocardial fibrosis was not increased in *Bcat2*$^{p.Q300*/p.Q300*}$ mice, minor structural remodelling within the AV-nodal area may still have impacted on AV-conduction.

Finally, the AV-nodal region is highly innervated and a modulatory role of BCAAs on neuronal function has been previously demonstrated in neurons,[35] providing another potential mechanism by which AV-conduction may have been affected. Interestingly, gender differences in electrophysiological effects of BCAAs appear to be present in both humans (**Table 1**) and mice (see **Suppl. Table S9**), which may be due to intrinsic BCAA concentration differences between men and women,[36] and/or gender-related differences in ion channels, exchangers and calcium handling.[37,38]

Importantly, the electrophysiological changes and pro-arrhythmic events observed in hPSC-CMs incubated with elevated BCAA levels confirm a direct pro-arrhythmic effect of BCAAs in cardiomyocytes. To date, *BCAT2* human mutations have been reported in only six individuals, associated mainly with developmental delay and autistic features.[39] Affected individuals displayed elevated plasma BCAA levels of up to 4 mmol/L (valine), with plasma BCKA levels remaining unchanged as in *Bcat2*$^{p.Q300*/p.Q300*}$ mice. Interestingly, valine levels were generally more elevated than leucine and isoleucine in *BCAT2* mutation carriers,[39,40] similar to our findings in *Bcat2*$^{p.Q300*/p.Q300*}$ mice. Valine appears to play a central role in BCAA-induced electrophysiological abnormalities, as evidenced by our findings in hPSC-CMs that increased levels of valine only were sufficient to induce pro-arrhythmic effects. Moreover, we observed the strongest correlation with ECG parameters for valine in the KORA cohort. While MSUD patients also have elevated BCAA plasma levels, arrhythmias have not been reported but cardiac electrophysiological assessment is likely not routinely performed. Similarly, arrhythmias have as yet not been reported in *BCAT2* mutation carriers, but our results suggests that an in-depth cardiac electrophysiological investigation and follow-up could be beneficial for these patients as well as individuals suffering MSUD.

Acute BCAA administration has been shown to reduce infarct size and exert cardioprotective effects during myocardial ischemia-reperfusion.[41] In contrast, chronic BCAA administration was found to exacerbate cardiac dysfunction and remodelling following myocardial infarction, and furthermore increased myocardial vulnerability to ischemia-reperfusion injury by enhancing glycolysis and fatty acid oxidation.[42,43] Taken together, these findings and our current observations suggest time-dependent effects triggered by BCAAs, with acute administration presenting potential benefits while a chronic exposure would be deleterious for cardiac (electrical) function. Crucially, we here demonstrate pro-arrhythmic actions of chronically elevated BCAA levels through direct effects on the cardiomyocyte level outside of the cardiac ischemia-reperfusion context.

The striking rapamycin-mediated reversal of pro-arrhythmic events in hPSC-CMs as well as the absence of effect of rapamycin in non-BCAA treated cells suggest a central role of mTOR on the electrophysiological dysfunctions triggered by elevated BCAAs. A number of studies have implicated increased reactive oxygen species (ROS)

production secondary to mTOR pathway activation in the detrimental effects of BCAAs supporting our current observations.[35,44] ROS-driven oxidative stress is known to induce pro-arrhythmic calcium dysregulation in cardiomyocytes as observed in our *Bcat2*$^{p.Q300*/p.Q300*}$ mice.[45] Interestingly, two recent studies have shown that low-BCAA diets can improve life-span through a decreased activation of the mTOR pathway, suggesting that dietary intervention could represent a preventive option in patients with elevated BCAA plasma levels.[46,47] The activation of the mTOR molecular pathway has also been linked to cardiac hypertrophy and structural remodelling.[48,49] While *Bcat2*$^{p.Q300*/p.Q300*}$ mice showed absence of fibrosis and normal cardiac dimensions, they did display increased ventricular transcript levels of *Anf*, indicating that pro-hypertrophic remodeling, likely secondary to mTOR pathway activation, preceded sudden death. We hypothesize that BCAA levels in affected mice rose drastically within a short period of time following weaning, causing severe electrophysiological changes and sudden death before more overt cardiac remodelling such as fibrosis could occur. BCAAs have also been shown to regulate AMP-activated protein kinase (AMPK),[25] which functions as a metabolic sensor in cardiomyocytes. Interestingly, AMPK can directly modulate sarcolemmal ion channels and transporters, providing an additional pathway through which BCAAs can impact on cardiomyocyte electrophysiology.[50,51] Crucially, the pro-arrhythmic potential of the clinically observed increased BCAA levels may be enhanced by conditions that further compromise either BCAA catabolism or cardiac conduction and repolarization, such as for instance metabolic disturbances, certain QT-prolonging drugs and structural alterations (cardiac hypertrophy, fibrosis). BCAA dysregulation is furthermore an increasingly recognized feature of diabetes mellitus, obesity and heart failure, acquired disorders associated with an increased risk for arrhythmias and SCD.[4–6,15–17,52] Our current observations suggest that enhanced BCAA plasma levels as observed in metabolic syndromes may underlie, at least in part, the increased susceptibility to cardiac arrhythmias and SCD observed in these patients, constituting a potential target for the prevention and treatment of cardiac arrhythmias in this setting.

LIMITATIONS

The ENU mutagenesis approach is a powerful tool for identifying potential novel genes and pathways, but is inherently limited by the fact that a potential role for additional ENU-induced mutations besides *Bcat2*$^{p.Q300*/p.Q300*}$ cannot be completely ruled out. Nevertheless, the sudden death phenotype remained after backcrossing the mice onto another genetic background, strengthening the involvement of the *Bcat2*$^{p.Q300*/p.Q300*}$ mutation. Importantly, the identification of the *Bcat2* mutation led to the discovery of elevated BCAA plasma levels in affected mice and the subsequent establishment of their pro-arrhythmic effects in an independent system (hPSC-CMs). While we were not able to establish whether *Bcat2*$^{p.Q300*/p.Q300*}$ mice died from cardiac arrhythmia (given the young age at which sudden death occurred), the robust arrhythmogenic electrophysiological

alterations in both *Bcat2*$^{p.Q300*/p.Q300*}$ mouse cardiomyocytes and hPSC-CMs incubated with elevated levels of BCAAs confirmed a pro-arrhythmic effect of the latter. *Bcat2*$^{p.Q300*/p.Q300*}$ mice presented with severely elevated BCAA levels whereas BCAA plasma levels in the KORA cohort were markedly lower. However, KORA participants provided a fasting blood sample, were not supplementing BCAAs for nutritional purposes, and were considered healthy (i.e. not metabolically compromised). Hence, even under normal circumstances in the general population, BCAAs are associated with cardiac conduction and repolarization. It will be an interesting future investigation to study if strongly increased BCAA levels in humans, as it is the case with nutritional supplementation or in the setting of metabolic disorders such as obesity or diabetes, result in even more pronounced ECG changes and/or arrhythmias. Milder elevations of BCAA levels following a longer exposure may also trigger cardiac structural remodelling through mTOR pathway activation. Both electrophysiological and structural consequences may be of significance in patients presenting an altered BCAA metabolism as well as in athletes supplementing their diet with BCAAs.

CONCLUSION

Using an unbiased approach, we have identified BCAA metabolism as a novel modulator of cardiac electrical function and a mediator of cardiac arrhythmias and sudden death. This new mechanism linking BCAAs to pro-arrhythmia may not only be relevant for inherited BCAT2 deficiency, but also for acquired metabolic disorders such as diabetes, obesity and heart failure in which BCAA metabolism is impaired. Since cellular BCAA metabolism is reflected by BCAA plasma levels, the latter may serve as a circulating prognostic biomarker of arrhythmia and SCD risk. Moreover, such metabolic mechanisms are modifiable through e.g. dietary interventions, providing novel preventive and therapeutic targets that overcome the drawbacks of conventional anti-arrhythmic approaches targeting ion channels or transporters. Additionally, we here provide the first proof of concept that pharmacological inhibition of the mTOR pathway can abolish the pro-arrhythmic events provoked by elevated BCAAs. Overall, our findings pave the way for novel research into therapeutic strategies aimed at preventing electrical dysfunction and arrhythmogenesis in patients suffering from diabetes, obesity and heart failure.

ACKNOWLEDGEMENTS

The authors thank Rianne Wolswinkel for expert technical assistance. The KORA study was initiated and financed by the Helmholtz Zentrum München – German Research Center for Environmental Health, which is funded by the German Federal Ministry of Education and Research (BMBF) and by the State of Bavaria. Furthermore, KORA

research was supported within the Munich Center of Health Sciences (MC-Health), Ludwig-Maximilian's-University, as part of LMUinnovativ. We also thank Professor Tim Claridge for use of the NMR facility, Department of Chemistry, University of Oxford.

SOURCES OF FUNDING

This work was supported by grants from the Dutch Heart Foundation (CVON-PREDICT2 and CVON-eDETECT; to Drs Bezzina and Remme), the Netherlands Organization for Scientific Research (Off Road fellowship, 451001031, to Dr Portero; VICI fellowship, 016.150.610, to Dr Bezzina; VIDI fellowship, 91714371, to Dr Remme), the Philippa and Marvin Carsley Chair in cardiology (Dr Tadros), a Fondation Leducq Transatlantic Network of Excellence (Drs Bezzina and Remme) and by the Medical Research Council, UK (MCU142684172 and MC_PC_13045, Dr Potter). Dr Tadros is a clinical research scholar of Fonds de recherche du Québec – Santé. Dr. Treur is supported by a 2019 NARSAD Young Investigator Grant from the Brain & Behavior Research Foundation.

AUTHOR CONTRIBUTION:

VP, CRB, PKP and CAR conceived and designed the project. PKP lead the early description of the sudden death phenotype and identification of mutants. TN performed the initial sudden death phenotypic characterisation and mutant characterisation. SF and AB carried out phenotypic analysis. IJC, FP and TAH acquired and analysed urinary and plasma NMR data. VP, SP, GAM, AB, SC, AOV performed electrophysiological measurements and data analysis. MFS, MWTT, VP, RT, JLT, MMN, GK, CG, AP, SK participated in the KORA data analysis. VP, TN and LB performed western blots and qPCR experiments. CRB, PKP and CAR supervised the project. VP, CRB, PKP and CAR wrote the manuscript. All co-authors critically revised the manuscript for intellectual content.

DISCLOSURES

None

REFERENCES

1. Deo R, Albert CM. Epidemiology and genetics of sudden cardiac death. *Circulation* 2012;125:620–637.
2. Priori SG, Blomström-Lundqvist C, Mazzanti A, Blom N, Borggrefe M, Camm J, Elliott PM, Fitzsimons D, Hatala R, Hindricks G, Kirchhof P, Kjeldsen K, Kuck K-H, Hernandez-Madrid A, Nikolaou N, Norekvål TM, Spaulding C, Veldhuisen DJ Van, ESC Scientific Document Group. 2015 ESC Guidelines for the management of patients with ventricular arrhythmias and the prevention of sudden cardiac death: The Task Force for the Management of Patients with Ventricular Arrhythmias and the Prevention of Sudden Cardiac Death of the European Society of Cardiology (ESC). Endorsed by: Association for European Paediatric and Congenital Cardiology (AEPC). *Eur Heart J* 2015;36:2793–2867.
3. Hoeijen DA Van, Blom MT, Bardai A, Souverein PC, Boer A De, Tan HL. Reduced pre-hospital and in-hospital survival rates after out-of-hospital cardiac arrest of patients with type-2 diabetes mellitus: an observational prospective community-based study. *Europace* 2015;17:753–760.
4. Jouven X, Lemaître RN, Rea TD, Sotoodehnia N, Empana J-P, Siscovick DS. Diabetes, glucose level, and risk of sudden cardiac death. *Eur Heart J* 2005;26:2142–2147.
5. Tomaselli GF, Zipes DP. What causes sudden death in heart failure? *Circ Res* 2004;95:754–763.
6. Finocchiaro G, Papadakis M, Dhutia H, Cole D, Behr ER, Tome M, Sharma S, Sheppard MN. Obesity and sudden cardiac death in the young: Clinical and pathological insights from a large national registry. *Eur J Prev Cardiol* 2018;25:395–401.
7. Huxley RR, Lopez FL, Folsom AR, Agarwal SK, Loehr LR, Soliman EZ, Maclehose R, Konety S, Alonso A. Absolute and attributable risks of atrial fibrillation in relation to optimal and borderline risk factors: the Atherosclerosis Risk in Communities (ARIC) study. *Circulation* 2011;123:1501–1508.
8. Wang TJ, Parise H, Levy D, D'Agostino RB, Wolf PA, Vasan RS, Benjamin EJ. Obesity and the risk of new-onset atrial fibrillation. *JAMA* 2004;292:2471–2477.
9. Adriaens ME, Lodder EM, Moreno-Moral A, Šilhavý J, Heinig M, Glinge C, Belterman C, Wolswinkel R, Petretto E, Pravenec M, Remme CA, Bezzina CR. Systems Genetics Approaches in Rat Identify Novel Genes and Gene Networks Associated With Cardiac Conduction. *J Am Heart Assoc* 2018;7:e009243.
10. Lodder EM, Scicluna BP, Milano A, Sun AY, Tang H, Remme CA, Moerland PD, Tanck MWT, Pitt GS, Marchuk DA, Bezzina CR. Dissection of a Quantitative Trait Locus for PR Interval Duration Identifies Tnni3k as a Novel Modulator of Cardiac Conduction. Barsh GS, ed. *PLoS Genet* 2012;8:e1003113.
11. Potter PK, Bowl MR, Jeyarajan P, Wisby L, Blease A, Goldsworthy ME, Simon MM, Greenaway S, Michel V, Barnard A, Aguilar C, Agnew T, Banks G, Blake A, Chessum L, Dorning J, Falcone S, Goosey L, Harris S, Haynes A, Heise I, Hillier R, Hough T, Hoslin A, Hutchison M, King R, Kumar S, Lad H V, Law G, MacLaren RE, et al. Novel gene function revealed by mouse mutagenesis screens for models of age-related disease. *Nat Commun* 2016;7:12444.

12. Arnold CN, Barnes MJ, Berger M, Blasius AL, Brandl K, Croker B, Crozat K, Du X, Eidenschenk C, Georgel P, Hoebe K, Huang H, Jiang Z, Krebs P, Vine D La, Li X, Lyon S, Moresco EMY, Murray AR, Popkin DL, Rutschmann S, Siggs OM, Smart NG, Sun L, Tabeta K, Webster V, Tomisato W, Won S, Xia Y, Xiao N, et al. ENU-induced phenovariance in mice: Inferences from 587 mutations. *BMC Res Notes* 2012;
13. Acevedo-Arozena A, Wells S, Potter P, Kelly M, Cox RD, Brown SDM. ENU Mutagenesis, a Way Forward to Understand Gene Function. *Annu Rev Genomics Hum Genet* 2008;
14. Riedl A, Wawro N, Gieger C, Meisinger C, Peters A, Roden M, Kronenberg F, Herder C, Rathmann W, Völzke H, Reincke M, Koenig W, Wallaschofski H, Hauner H, Daniel H, Linseisen J. Identification of Comprehensive Metabotypes Associated with Cardiometabolic Diseases in the Population-Based KORA Study. *Mol Nutr Food Res* 2018;62:e1800117.
15. She P, Horn C Van, Reid T, Hutson SM, Cooney RN, Lynch CJ. Obesity-related elevations in plasma leucine are associated with alterations in enzymes involved in branched-chain amino acid metabolism. *Am J Physiol Endocrinol Metab* 2007;293:E1552-63.
16. Würtz P, Tiainen M, Mäkinen V-P, Kangas AJ, Soininen P, Saltevo J, Keinänen-Kiukaanniemi S, Mäntyselkä P, Lehtimäki T, Laakso M, Jula A, Kähönen M, Vanhala M, Ala-Korpela M. Circulating metabolite predictors of glycemia in middle-aged men and women. *Diabetes Care* 2012;35:1749–1756.
17. Ruiz-Canela M, Guasch-Ferré M, Toledo E, Clish CB, Razquin C, Liang L, Wang DD, Corella D, Estruch R, Hernáez Á, Yu E, Gómez-Gracia E, Zheng Y, Arós F, Romaguera D, Dennis C, Ros E, Lapetra J, Serra-Majem L, Papandreou C, Portoles O, Fitó M, Salas-Salvadó J, Hu FB, Martínez-González MA. Plasma branched chain/aromatic amino acids, enriched Mediterranean diet and risk of type 2 diabetes: case-cohort study within the PREDIMED Trial. *Diabetologia* 2018;61:1560–1571.
18. Veerman CC, Kosmidis G, Mummery CL, Casini S, Verkerk AO, Bellin M. Immaturity of Human Stem-Cell-Derived Cardiomyocytes in Culture: Fatal Flaw or Soluble Problem? *Stem Cells Dev* 2015;
19. Verkerk AO, Veerman CC, Zegers JG, Mengarelli I, Bezzina CR, Wilders R. Patch-clamp recording from human induced pluripotent stemcell-derived cardiomyocytes: Improving action potential characteristics throughdynamic clamp. *Int J Mol Sci* 2017;
20. Meijer van Putten RME, Mengarelli I, Guan K, Zegers JG, Ginneken ACG van, Verkerk AO, Wilders R. Ion channelopathies in human induced pluripotent stem cell derived cardiomyocytes: a dynamic clamp study with virtual IK1. *Front Physiol* Frontiers Media SA; 2015;6:7.
21. Portero V, Casini S, Hoekstra M, Verkerk AO, Mengarelli I, Belardinelli L, Rajamani S, Wilde AAM, Bezzina CR, Veldkamp MW, Remme CA. Anti-arrhythmic potential of the late sodium current inhibitor GS-458967 in murine Scn5a-1798insD+/– and human SCN5A-1795insD+/– iPSC-derived cardiomyocytes. *Cardiovasc Res* 2017;113:829–838.
22. Baartscheer A, Schumacher CA, Fiolet JWT. Cytoplasmic sodium, calcium and free energy change of the Na+/Ca2+-exchanger in rat ventricular myocytes. *J Mol Cell Cardiol* 1998;
23. Baartscheer A, Schumacher CA, Belterman CNW, Coronel R, Fiolet JWT. SR calcium handling and calcium after-transients in a rabbit model of heart failure. *Cardiovasc Res* 2003;

24. Holeček M. Branched-chain amino acids in health and disease: metabolism, alterations in blood plasma, and as supplements. *Nutr Metab (Lond)* 2018;15:33.
25. Wang XJ, Yang X, Wang RX, Jiao HC, Zhao JP, Song ZG, Lin H. Leucine alleviates dexamethasone-induced suppression of muscle protein synthesis via synergy involvement of mTOR and AMPK pathways. *Biosci Rep* 2016;36:e00346–e00346.
26. Neinast M, Murashige D, Arany Z. Branched Chain Amino Acids. *Annu Rev Physiol* 2018;81:annurev-physiol-020518-114455.
27. Sciarretta S, Volpe M, Sadoshima J. Mammalian target of rapamycin signaling in cardiac physiology and disease. *Circ Res* 2014;114:549–564.
28. Wu JY, Kao HJ, Li SC, Stevens R, Hillman S, Millington D, Chen YT. ENU mutagenesis identifies mice with mithochondrial branched-chain aminotransferase deficiency resembling human maple syrup urine disease. *J Clin Invest* The American Society for Clinical Investigation; 2004;113:434–440.
29. She P, Reid TM, Bronson SK, Vary TC, Hajnal A, Lynch CJ, Hutson SM. Disruption of BCATm in Mice Leads to Increased Energy Expenditure Associated with the Activation of a Futile Protein Turnover Cycle. *Cell Metab* 2007;
30. Hutson SM, Wallin R, Hall TR. Identification of mitochondrial branched chain aminotransferase and its isoforms in rat tissues. *J Biol Chem* 1992;267:15681–15686.
31. Drown PM, Torres N, Tovar AR, Davoodi J, Hutson SM. Use of sulfhydryl reagents to investigate branched chain α-keto acid transport in mitochondria. *Biochim Biophys Acta - Biomembr* Biochim Biophys Acta; 2000;1468:273–284.
32. Nickel AG, Hardenberg A Von, Hohl M, Löffler JR, Kohlhaas M, Becker J, Reil JC, Kazakov A, Bonnekoh J, Stadelmaier M, Puhl SL, Wagner M, Bogeski I, Cortassa S, Kappl R, Pasieka B, Lafontaine M, Lancaster CRD, Blacker TS, Hall AR, Duchen MR, Kästner L, Lipp P, Zeller T, Müller C, Knopp A, Laufs U, Böhm M, Hoth M, Maack C. Reversal of mitochondrial transhydrogenase causes oxidative stress in heart failure. *Cell Metab* Cell Press; 2015;22:472–484.
33. Eisner DA, Caldwell JL, Trafford AW, Hutchings DC. The Control of Diastolic Calcium in the Heart: Basic Mechanisms and Functional Implications. Circ. Res. Lippincott Williams and Wilkins; 2020. p. 395–412.
34. Rivaud MR, Marchal GA, Wolswinkel R, Jansen JA, Made I Van Der, Beekman L, Ruiz-Villalba A, Baartscheer A, Rajamani S, Belardinelli L, Veen TAB Van, Basso C, Thiene G, Creemers EE, Bezzina CR, Remme CA. Functional modulation of atrio-ventricular conduction by enhanced late sodium current and calcium-dependent mechanisms in Scn5a1798insD/+mice. *Europace* Oxford University Press; 2020;22:1579–1589.
35. Caioli S, Candelotti E, Pedersen JZ, Saba L, Antonini A, Incerpi S, Zona C. Baicalein reverts L-valine-induced persistent sodium current up-modulation in primary cortical neurons. *Biochim Biophys Acta* 2016;1862:566–575.
36. Zhao X, Han Q, Liu Y, Sun C, Gang X, Wang G. The Relationship between Branched-Chain Amino Acid Related Metabolomic Signature and Insulin Resistance: A Systematic Review. J. Diabetes Res. Hindawi Limited; 2016.

37. Tadros R, Ton AT, Fiset C, Nattel S. Sex differences in cardiac electrophysiology and clinical arrhythmias: Epidemiology, therapeutics, and mechanisms. Can. J. Cardiol. Pulsus Group Inc.; 2014. p. 783–792.
38. Parks RJ, Howlett SE. Sex differences in mechanisms of cardiac excitation-contraction coupling. Pflugers Arch. Eur. J. Physiol. Pflugers Arch; 2013. p. 747–763.
39. Knerr I, Colombo R, Urquhart J, Morais A, Merinero B, Oyarzabal A, Pérez B, Jones SA, Perveen R, Preece MA, Rogers Y, Treacy EP, Mayne P, Zampino G, MacKinnon S, Wassmer E, Yue WW, Robinson I, Rodríguez-Pombo P, Olpin SE, Banka S. Expanding the genetic and phenotypic spectrum of branched-chain amino acid transferase 2 (BCAT2) deficiency. *J Inherit Metab Dis* 2019;
40. Wang XL, Li CJ, Xing Y, Yang YH, Jia JP. Hypervalinemia and hyperleucine-isoleucinemia caused by mutations in the branched-chain-amino-acid aminotransferase gene. *J Inherit Metab Dis* 2015;
41. Satomi S, Morio A, Miyoshi H, Nakamura R, Tsutsumi R, Sakaue H, Yasuda T, Saeki N, Tsutsumi YM. Branched-chain amino acids-induced cardiac protection against ischemia/ reperfusion injury. *Life Sci* Elsevier Inc.; 2020;245.
42. Li Y, Xiong Z, Yan W, Gao E, Cheng H, Wu G, Liu Y, Zhang L, Li C, Wang S, Fan M, Zhao H, Zhang F, Tao L. Branched chain amino acids exacerbate myocardial ischemia/ reperfusion vulnerability via enhancing GCN2/ATF6/PPAR-α pathway-dependent fatty acid oxidation. *Theranostics* Ivyspring International Publisher; 2020;10:5623–5640.
43. Wang W, Zhang F, Xia Y, Zhao S, Yan W, Wang H, Lee Y, Li C, Zhang L, Lian K, Gao E, Cheng H, Tao L. Defective branched chain amino acid catabolism contributes to cardiac dysfunction and remodeling following myocardial infarction. *Am J Physiol - Hear Circ Physiol* American Physiological Society; 2016;311:H1160–H1169.
44. Zhenyukh O, Civantos E, Ruiz-Ortega M, Sánchez MS, Vázquez C, Peiró C, Egido J, Mas S. High concentration of branched-chain amino acids promotes oxidative stress, inflammation and migration of human peripheral blood mononuclear cells via mTORC1 activation. *Free Radic Biol Med* 2017;104:165–177.
45. Bertero E, Maack C. Calcium signaling and reactive oxygen species in Mitochondria. Circ. Res. Lippincott Williams and Wilkins; 2018. p. 1460–1478.
46. Lu J, Temp U, Müller-Hartmann A, Esser J, Grönke S, Partridge L. Sestrin is a key regulator of stem cell function and lifespan in response to dietary amino acids. *Nat Aging* Springer Science and Business Media LLC; 2021;1:60–72.
47. Richardson NE, Konon EN, Schuster HS, Mitchell AT, Boyle C, Rodgers AC, Finke M, Haider LR, Yu D, Flores V, Pak HH, Ahmad S, Ahmed S, Radcliff A, Wu J, Williams EM, Abdi L, Sherman DS, Hacker TA, Lamming DW. Lifelong restriction of dietary branched-chain amino acids has sex-specific benefits for frailty and life span in mice. *Nat Aging* Springer Science and Business Media LLC; 2021;1:73–86.
48. Zhang D, Contu R, Latronico MVG, Zhang JL, Rizzi R, Catalucci D, Miyamoto S, Huang K, Ceci M, Gu Y, Dalton ND, Peterson KL, Guan KL, Brown JH, Chen J, Sonenberg N, Condorelli G. MTORC1 regulates cardiac function and myocyte survival through 4E-BP1 inhibition in mice. *J Clin Invest* The American Society for Clinical Investigation; 2010;120:2805–2816.

49. Shioi T, McMullen JR, Tarnavski O, Converso K, Sherwood MC, Manning WJ, Izumo S. Rapamycin attenuates load-induced cardiac hypertrophy in mice. *Circulation* Lippincott Williams & Wilkins; 2003;107:1664–1670.
50. Harada M, Tadevosyan A, Qi X, Xiao J, Liu T, Voigt N, Karck M, Kamler M, Kodama I, Murohara T, Dobrev D, Nattel S. Atrial Fibrillation Activates AMP-Dependent Protein Kinase and its Regulation of Cellular Calcium Handling: Potential Role in Metabolic Adaptation and Prevention of Progression. *J Am Coll Cardiol* 2015;66:47–58.
51. Andersen MN, Skibsbye L, Tang C, Petersen F, MacAulay N, Rasmussen HB, Jespersen T. PKC and AMPK regulation of Kv1.5 potassium channels. *Channels (Austin)* 2015;9:121–128.
52. Sun H, Olson KC, Gao C, Prosdocimo DA, Zhou M, Wang Z, Jeyaraj D, Youn J-Y, Ren S, Liu Y, Rau CD, Shah S, Ilkayeva O, Gui W-J, William NS, Wynn RM, Newgard CB, Cai H, Xiao X, Chuang DT, Schulze PC, Lynch C, Jain MK, Wang Y. Catabolic Defect of Branched-Chain Amino Acids Promotes Heart Failure. *Circulation* 2016;133:2038–2049.

SUPPLEMENTAL MATERIAL

EXPANDED MATERIALS & METHODS

Pyrosequencing

DNA was extracted from mouse ear biopsies using Kapa express extract (Sigma Aldrich). PCR was performed (Taq PCR master mix – Qiagen) focused on a region surrounding each mutation with biotinylated reverse primers (*Bcat2* F – GTAACCCCCCCACTGAAT, *Bcat2* R – AACTCACCCCAAGTCCTG, *Siglech* F – ACGACCACACTCTCCTCAG, *Siglech* R – AGGTGACATTGAGCTGGATAG). Following PCR, the biotinylated strand was isolated by denaturation and washing, and pyrosequencing performed (PSQ HS96A pyrosequencer, Pyromark reagents). Sequencing primers are added (*Bcat2* – TGCCTGGAGTAGTTCG, *Siglech* - AACCAACCTCACCTGT) as well as enzyme and substrate (Qiagen). Successive addition of nucleotides provides a luminescent signal incorporated into the DNA strand through synthesis. Pyrosequencing results are presented in **Suppl. Fig. S1**.

NMR methodology

Urinary NMR analysis

Free-fed mouse urine samples were collected by metabolic caging overnight and stored at -80 °C the following day until NMR analysis. Urinary samples were collected from two batches of mice. Firstly, batch A from the initial ENU screen and secondly, batch B from the *Bcat2* backcrossed congenic line. From batch A, 18 urine samples were collected (*Bcat2*$^{+/+}$, n=10, mean (range) age 4.31 (4.29-4.57) weeks; *Bcat2*$^{p.Q300*/p.Q300*}$, n=8, mean (range) age 4.10 (4.00-4.29) weeks) and analysed using a JEOL Eclipse+ 500MHz NMR system housed at MRC Harwell. From batch B, 10 urine samples from the congenic line mice were collected (*Bcat2*$^{+/+}$, n=5, mean (range) age 4.03 (3.86-4.14) weeks; *Bcat2*$^{p.Q300*/p.Q300*}$, n=5, mean (range) age 4.14 (4.14) weeks) and subsequently analysed using a Bruker AV 700 MHz NMR system at the Department of Chemistry, University of Oxford. Both female and male mice were included in the NMR urinary BCAA quantification.

In preparation for NMR analyses, the urine samples were briefly thawed at room temperature and centrifuged at 8,000 rpm for 2 minutes. A urine volume was mixed with sterile water and 0.2M phosphate buffer (pH7.4, containing 20% D_2O to provide an NMR field frequency lock and 1 mM trimethylsilyl-propionic acid (TSP) for internal chemical shift reference at 0.00 ppm) in the proportions 1:2:3. At 500 MHz and 700 MHz, 100 µl was diluted and buffered to a volume of 600 µl, and 550 µl of this buffered urine was analysed in a 5 mm NMR tube. Water pre-saturation was used for all data acquisitions. The spectral width was 15ppm, pulse angle 90°, acquisition time 4.36s, relaxation delay 2s and constant receiver gain. The free induction decay was zero filled and multiplied by an exponential function of 0.3Hz line broadening prior to Fourier Transformation. The NMR spectra were manually phased using proprietary software.

NMR spectral resonances were assigned according to the literature.[1] The BCAA region was integrated relative to the total signal intensity in the region (3.50-1.07 ppm).

NMR plasma sample preparation and analysis

Plasma samples were collected from 27 free-fed *Bcat2* backcrossed congenic line (*Bcat2*$^{+/+}$, n=11, mean (range) age 4.83 (4.71-5.00) weeks; *Bcat2*$^{+/p.Q300*}$, n=9, mean (range) age 4.90 (4.71-5.00) weeks; *Bcat2*$^{p.Q300*/p.Q300*}$, n=7, mean (range) age 4.88 (4.71-5.00) weeks). All plasma samples were stored at -80°C until NMR analysis. Both female and male mice were included in the NMR plasmatic BCAA quantification.

In preparation for proton (^{1}H)-NMR spectroscopy studies, plasma aliquots were thawed at 4 °C for 20 min and centrifuged for 5 min at 520 x g. A plasma volume of 100 µl was mixed with 100 µl D_2O, which provided an NMR field frequency lock and the plasma solution was transferred to a 3 mm OD NMR tube (Norell®, USA). All plasma (^{1}H)-NMR spectra were collected at 37°C using a Bruker AV 700 MHz NMR spectrometer housed in the Department of Chemistry, University of Oxford. NMR data were obtained using pulse-collect and spin-echo sequences. (^{1}H)-NMR spectra were acquired using both noesygppr1d pulse-collect and Carr-Purcell-Meiboom-Gill (CPMG) spin-echo sequences, each with 32 data collects, acquisition time 1.46 s, relaxation delay 2 s and a fixed receiver gain. The resulting free induction decay was zero filled by a factor of 2 and multiplied by an exponential function corresponding to 0.3 Hz line broadening prior to Fourier Transformation. The (^{1}H)-NMR spectra were manually phased using the Bruker TopSpin software (version 3.5 pl 5, Bruker Biospin Corporation, Billerica MA 01821) and referenced with the lactate doublet set to 1.33 ppm. (^{1}H)-NMR spectral resonances were assigned according to the literature.[2] Peaks in the BCAA region, 1.06 - 0.92 ppm, were assigned to valine, isoleucine and leucine (domain 10). The entire NMR spectrum was binned into regions of 0.02 ppm and integrated by the ACD/NMR Processor Academic Edition (version 12.01, Advanced Chemistry Development, Inc.)

Estimate of relative contribution of plasmatic valine, isoleucine and leucine in a representative pulse-collect NMR spectrum at 700 MHz from Bcat2$^{p.Q300*/p.Q300*}$

Peaks were initially manually integrated in more detail from one representative plasma pulse-collect NMR spectrum from a *Bcat2*$^{p.Q300*/p.Q300*}$ mouse using the Bruker TopSpin software integration routine. Appreciating the problems of peak overlap not only within the BCAA region, but also of overlap of the BCAA region with the lipid-CH_3 peak and with any broad underlying lipoprotein resonances, in the NMR spectrum selected, the estimate of valine:isoleucine:leucine peak integrals was 1:0.75:0.45.

Estimate of plasmatic valine concentration from CPMG spin-echo NMR spectra

Using NMR data collected using the CPMG spin-echo sequence (to minimise overlap from lipid and lipoprotein signals) the NMR doublet at 1.06-1.02 ppm was assigned to a CH_3 doublet of valine. The peak area of this region was compared to the signal level in

the region 5.24-5.22 ppm, which was assigned to the alpha-anomeric proton of glucose. The valine signal was divided by 3, to correct for the number of protons contributing to this doublet. Assuming α-β anomeric equilibrium, the area integration of the alpha-anomeric proton was divided by 0.36.[3] Similar spin-spin relaxation NMR values for the valine CH_3 doublet and the anomeric glucose peak were assumed. Finally, assuming a glucose concentration of 17 mM, on the basis of archived clinical chemistry data for *Bcat2*$^{p.Q300*/p.Q300*}$ mice, the concentration of valine was calculated from the valine CH_3 signal area relative to the glucose α-CH signal area using a correction factor of (0.36/3) *17.0 = 2.04.

Estimate of plasmatic xleucine concentration

Since the NMR resonances from leucine and isoleucine (xleucine) overlap in the region 0.97-0.92 ppm,[4] it is difficult to separate the contribution of these metabolites without the use of two-dimensional NMR techniques. Given that only one-dimensional NMR data were acquired, the xleucine concentration was estimated from the integral of the region 0.98-0.92ppm, divided by 4.5 (averaging the contribution of three protons to the isoleucine peak and six protons for the leucine peaks) and compared to the glucose anomeric doublet.

Biochemical screen

Further analysis of plasma was carried out by the clinical chemistry analysis of terminal plasma samples to determine if there were any other potential indicators of ill health; parameters measured are listed in **Suppl. Table S1**. Both female and male mice were included in the chemical chemistry screen. Clinical chemistry analysis was carried out on a Beckman Coulter AU680 analyser on terminal blood samples, acquired via retro-orbital bleeds into lithium heparin tubes under terminal anaesthesia. Blood samples were centrifuged at 5,000 x g for 10 minutes at 8°C and the resulting plasma was stored at -20°C prior to analysis. All analysis was carried out blinded using coded tubes.

Cardiac structural abnormalities

To assess the presence of cardiac hypertrophy, heart weight/body weight and heart weight/tibia length ratios were calculated. Histological assessment of cardiac tissue was carried out on haematoxylin and eosin (H&E) stained tissue obtained from 6-week-old G3 mice. Both female and male mice were included in the quantification.

mRNA expression analysis

Total RNA was extracted from ventricular tissue with Trizol (Sigma) following manufacturer's recommendations and stored at -80°C. 1000 ng of isolated RNA was reverse-transcribed into cDNA with Superscript II (Invitrogen) and Oligo(dT) primers. mRNA expression of *Anf, Slc8a1, Atp2a2 and Hprt* (primer sequences: *Hprt*-forward: 5'_CTTTCCCTGGTTAAGCAGTACAG_3', *Hprt*-reverse: 5'_GTCAAGGGCATATCCAACAACAAAC_3'; *Atp2a2*-forward: 5'_

TCCATCTGCTTGTCCATGTCAC_3', *Atp2a2*-reverse: 5'_GGAGCAGGAAGATTTGGTGGC_3', *Slc8a1*-forward: 5'_CCAACAGCTGGAGAGAGCAG_3', *Slc8a1*-reverse: 5'_GTAATCAAAACAGGAGGGCAGC_3'; *Anf*-forward: 5'_TTCCTCGTCTTGGCCTTTTG_3', *Anf*-reverse: 5'_CCTCATCTTCTACCGGCATC_3') was determined by RT-qPCR using SYBR Green (Roche) on the LightCycler 480 PCR system (Roche). Samples were first denatured at 95°C (5 minutes), followed by 45 cycles with denaturation at 95°C (10 seconds), annealing at 60°C (20 seconds), and extension at 72°C (20 seconds), followed by with a standard melting curve protocol. Melting curve analysis (LightCycler480, Roche) and size fractionation by agarose gel electrophoresis were used to confirm amplification of the expected product. The *Anf, Slc8a1, Atp2a2 and Hprt* transcript levels for each sample were analysed in triplicate using LinRegPCR.[5,6] *Hprt* served as a reference gene for normalization.

Surface ECG measurements

Mice were anesthetized by isoflurane inhalation (4% for induction, 0.8-1.5 % volume in oxygen for maintenance). Surface ECG recordings were performed for 5 min in mice in the prone position with limb 23-gauge needle using the Powerlab acquisition system (ADInstruments). ECG analysis was done with LabChart7Pro software (ADInstruments). The signal average ECG (SAECG) was calculated for leads I and II and manually analysed for ECG indices (P-, PR-, QRS-, and QT-duration and heart rate, HR). The following formula was used to correct QT-intervals for RR-interval: $QTc = QT/(RR/100)^{1/2}$. Finally, the averages of obtained SAECG parameters from lead I were calculated. Both female and male mice were included.

Cardiac arrhythmia inducibility

Mice were sacrificed by cervical dislocation after CO_2 exposure. The excised heart was cannulated, placed on a Langendorff perfusion set-up, and perfused at 37°C with Tyrode's solution (128 mmol/l NaCl, 4.7 mmol/l KCl, 1.45 mmol/l $CaCl_2$, 0.6 mmol/l $MgCl_2$, 27 mmol/l $NaHCO_3$, 0.4 mmol/l NaH2PO_4, and 11 mmol/l glucose [pH maintained at 7.4 by equilibration with a mixture of 95% O_2 and 5% CO_2]). Atria and ventricles were stimulated at a basic cycle length (BCL) of 120 ms (2 ms pulse duration, twice diastolic threshold). Inducibility of arrhythmias was evaluated using up to 3 extrastimuli (S1-S2-S3) (after 16 stimuli at BCL 120 ms), with progressively shortened coupling intervals of 10 ms until the capture was lost. Moreover, burst pacing was applied using 36 stimuli at BCL, followed by 40 shortly coupled stimuli at progressively shortened coupling intervals. Both female and male mice were included.

Optical mapping measurements

Optical mapping was carried out as previously described.[7] Following excision and cannulation as described above, hearts were incubated in 10 ml Tyrode's solution containing 15 µM Di-4 ANEPPS and mounted on an optical mapping setup and perfused at 37°C with Tyrode's solution. To prevent movement artifacts, blebbistatin was added

to Tyrode's solution. Excitation light was generated by a 5-watt power LED lamp (filtered 510 ± 20 nm). Fluorescence (filtered >610 nm) was transmitted through a tandem lens system on CMOS sensor (100 × 100 elements; MICAM Ultima). Pacing was performed at a BCL of 120 ms at twice the diastolic stimulation threshold from the center of the ventricular epicardial surface. Optical action potentials were analyzed, and local activation defined as the maximum positive slope of the action potential was calculated using custom software. Measured local activation times were used to construct ventricular activation maps. To calculate conduction velocity (CV) in longitudinal and transversal directions, the difference in activation time was determined between at least three consecutive electrode terminals parallel (longitudinal) or perpendicular (transversal) to the direction of propagation, as seen in isochronal maps. Three calculated parallel values of CV in each of the two directions were averaged. Both female and male mice were included.

Cardiomyocyte isolation

Mouse hearts were excised, cannulated, and mounted on a Langendorff set-up (see above), and perfused at 37 °C for 8 min with normal Tyrode's solution containing (in mmol/l): 140 NaCl, 5.4 KCl, 1.8 $CaCl_2$, 1.0 $MgCl_2$, 5.5 glucose, 5 HEPES; pH 7.4 (NaOH). Next, the heart was perfused for 8 minutes with a similar solution in which the calcium concentration was lowered to 1.08×10^{-5} mol/L (low calcium solution), and the enzymes Liberase Blendzyme type 4 (Roche Diagnostics, GmbH, Mannheim, Germany) and Elastase from porcine pancreas (SERVA Electrophoresis GmbH, Heidelberg, Germany) were added at a concentration of 0.055 and 0.008 mg/mL, respectively. Then, digested tissue was gently triturated in the low-calcium solution and single cardiomyocytes were washed twice in the low-calcium solution supplemented with BSA (1 mg/ml), and twice in normal Tyrode's solution at 37 °C. Cells were stored at room temperature and used within 4 h. Only male mice were included in the cellular electrophysiological studies.

Action potential measurements

Action potentials (APs) were measured at 36 °C using normal Tyrode's solution and were elicited at 2 Hz. Pipettes were filled with (in mmol/l): 125 K-gluconate, 20 KCl, 5 NaCl, 0.22 amphotericin-B, 10 HEPES, pH 7.2 (KOH). APs were elicited at 2 Hz by 2-ms, ≈1.2× threshold current pulses through the patch pipette. In single hPSC-CMs, APs were measured with similar conditions as for mouse cardiomyocytes, with the exception that the amount of amphotericin was doubled. Typically, hPSC-CMs have a small or even complete lack of the inward rectifying potassium current (I_{K1}). Consequently, hPSC-CMs have a depolarized resting membrane potential (RMP) and are frequently spontaneously active.[8] To overcome these conditions, we injected an *in silico* I_{K1} with kinetics of Kir2.1 channels through dynamic clamp,[9] as previously described and validated.[10,11] Consequently, cells became quiescent with a RMP of around −82 mV and APs were elicited at 1 Hz by 3 ms, ≈1.2-times the threshold current pulses through the patch pipette. Signals were low-pass filtered with a cut-off frequency of 5 kHz and digitized at

40 kHz. We analysed RMP, AP amplitude (APA), maximal AP upstroke velocity (V_{max}) and APD at 20, 50, and 90% repolarization (APD_{20}, APD_{50}, and APD_{90}, respectively). Data from 10 consecutive APs were averaged and potentials were corrected for the calculated liquid junction potential (15 mV). The fast pacing protocol used to count and quantify early after depolarizations (EADs), delayed after depolarizations (DADs) and triggered action potentials (TAPs) consisted in applying 20 pulse at a frequency of 5 Hz followed by a 10 second pause. The results were normalized per trace using 5 consecutive traces.

Sodium current measurements

The sodium current (I_{Na}) was measured using the ruptured patch-clamp technique. Glass pipettes were filled with a solution containing (in mmol/l): 3.0 NaCl, 133 CsCl, 2.0 $MgCl_2$, 2.0 Na_2ATP, 2.0 TEACl, 10.0 EGTA, 5.0 HEPES; pH 7.2 (CsOH). I_{Na} peak measurements were performed in a bath solution containing (in mmol/l): 7.0 NaCl, 133 CsCl, 1.8 $CaCl_2$, 1.2 $MgCl_2$, 11.0 glucose, HEPES 5.0, nifedipine 0.005; pH 7.4 (CsOH). For late I_{Na} measurements, we replaced 123 mmol/l CsCl by NaCl. Series resistance and cell membrane capacitance were compensated for 80-90%. Signals were filtered at 5 kHz and digitized at 40 kHz. Peak I_{Na} was measured at room temperature (21°C) from a holding potential of -120 mV following steps of 5 mV from -130 mV to +30 mV, with a cycle length of 5 s (**Suppl. Fig. S7C**). I_{Na} was defined as the difference between peak current and steady-state current. I_{Na} density was calculated by dividing current amplitude by cell membrane capacitance (C_m). C_m was determined by dividing the decay time constant of the capacitive transient in response to 5 mV hyperpolarizing steps from −40 mV, by the series resistance (Rs). Steady-state activation and inactivation curves were fitted using the Boltzmann equation $I/I_{max}=A/\{1.0+\exp[(V_{1/2}-V)/k]\}$ to determine $V_{1/2}$ (membrane potential for the half-maximal (in)activation) and the slope factor k. Late I_{Na} were measured at 36 °C as TTX (30 µM)-sensitive current using a descending ramp protocol (**Supplemental Figure S7A**).

Western blot analysis of WT and p.Q300* BCAT2 protein expression

Full length cDNA clone of BCAT2 (Dharmacon) was ligated into pCMV6-AN-Myc vector (Origene) using the restriction enzyme sites SgfI and AscI. The ligated vector was propagated in Xl-10 gold *E.coli* (Agilent) and extracted using plasmid midi kit (Qiagen). The C1121T mutation was introduced by Q5 site directed mutagenesis (NEB) using the following primers (5'>3'): GAGTAGTTCGATAAAGTCTGCTG and CAGGCAAGATGACGCCAT. Plasmid DNA was transfected using JetPRIME transfection reagent (Polyplus transfection) into HEK293T cells grown in DMEM (High glucose, Glutamax) supplemented with 10% FBS and penicillin/streptomycin according to manufacturer's instructions. 48 hours following transfection cells were lysed in 200µl of 1x LDS sample buffer (invitrogen) containing protease inhibitors (Roche). 10µl of cell lysate was loaded into a 4-12% bis-tris gels (Invitrogen) and run in 1xMOPS buffer. Proteins were transferred to PVDF membrane (GE Healthcare) in 1x NuPAGE transfer buffer (Invitrogen), 20% methanol, and NuPAGE antioxidant (Invitrogen) at 30 volts for 60 minutes. The membrane was

blocked in 5% milk in PBS containing 0.1% tween for 1 hour, and primary antibody (Mouse anti-Myc 1:1000 – Origene) incubated overnight in 5% milk PBS-tween at 4°C. Following overnight incubation, the membrane was washed in PBS-tween and incubated in secondary antibody (goat anti-mouse IgG IRdye800CW 1:15000 – Li-COR) for 1 hour at room temperature. Signal was visualised on Li-Cor ClX scanner.

Association between plasma BCAA levels and ECG measures in the KORA F4 Study

KORA cohort description

The community-based KORA Study (Cooperative Health Research in the Augsburg Region) is conducted in Augsburg, Southern Germany. The KORA F4 Study recruited 3080 participants between 2006 and 2008.[12] All individuals received a detailed characterization of demographic information and comorbid conditions. Peripheral blood from fasting individuals was drawn for biomarker analyses. In addition, all participants obtained a standard 12-lead electrocardiogram (ECG) after 10 minutes rest in supine position using the Hannover ECG System (HES, Hannover, Germany). For the current analysis, we used heart rate, PR interval, QRS duration, and the QTc interval, corrected using Bazett's formula. All study participants provided written informed consent; the study was approved by the Bayerische Landesärztekammer.

Branched-chain amino acid assessment

All participants underwent metabolic profiling using the Biocrates AbsoluteIDQp150 kit (Biocates Life Sciences AG, Innsbruck, Austria), adhering to manufacturer recommendations as previously described.[12] For the current analysis, we extracted µmol/L concentrations of the BCAAs valine and xleucine (i.e. the combination of leucine and isoleucine).

KORA statistical analysis

Of 3080 KORA F4 participants, 75 were excluded due to unavailability or non-interpretability of ECGs, or absence of sinus rhythm. An additional 109 individuals were excluded following quality control of metabolite measurements, leaving 2896 samples for analysis. To account for the known interaction of BCAA plasma concentrations with body weight and age, we restricted our cohort to participants ≥50 kg and ≤70 years of age. Given the interference of the anti-diabetic drug metformin with BCAA concentrations, we further excluded participants with diabetes mellitus. In summary, additional 592 participants were excluded, leaving 2304 individuals in the final data set. To determine a relation between ECG measures and BCAAs, we fitted linear regression models adjusting for sex. To rule out interactions with age or sex, we tested for statistical interaction by including multiplicative interaction terms. As we found no evidence of interaction, interaction terms were removed from the final models. All statistical analyses in KORA were performed using STATA 12.0 (StataCorp LP, College Station, TX, USA).

Statistical analysis

No statistical methods were used to predetermine sample size. Differences between two unpaired groups were assessed using two-tailed *t*-tests when following a normal distribution and Mann-Whitney Rank sum test if normality test failed. All statistical tests were performed using sigma stat 3.5 software (Systat Software, Inc). Variability in all plots and graphs is presented as the s.e.m. All $P < 0.05$ were considered to be significant. *$P < 0.05$; **$P \leq 0.01$; #$P \leq 0.001$. Summary statistics are depicted in **Suppl. Tables S2-5**.

REFERENCES

1. Wishart DS, Tzur D, Knox C, Eisner R, Guo AC, Young N, Cheng D, Jewell K, Arndt D, Sawhney S, et al. HMDB: the Human Metabolome Database. *Nucleic Acids Res*. 2007;35:D521-526.
2. Psychogios N, Hau DD, Peng J, Guo AC, Mandal R, Bouatra S, Sinelnikov I, Krishnamurthy R, Eisner R, Gautam B, et al. The human serum metabolome. *PLoS ONE*. 2011;6:e16957.
3. Ando I, Hirose T, Nemoto T, Totsune K, Imai Y, Takeuchi K, Fujiwara M. Quantification of molecules in (1)H-NMR metabolomics with formate as a concentration standard. *J Toxicol Sci*. 2010;35:253–256.
4. Ghosh S, Sengupta A, Chandra K. Quantitative metabolic profiling of NMR spectral signatures of branched chain amino acids in blood serum. *Amino Acids*. 2015;47:2229–2236.
5. Ramakers C, Ruijter JM, Lekanne Deprez RH, Moorman AFM. Assumption-free analysis of quantitative real-time polymerase chain reaction (PCR) data. *Neurosci Lett*. 2003;339:62–66.
6. Ruijter JM, Ramakers C, Hoogaars WMH, Karlen Y, Bakker O, van den hoff MJB, Moorman AFM. Amplification efficiency: Linking baseline and bias in the analysis of quantitative PCR data. *Nucleic Acids Res*. 2009;37.
7. Rivaud MR, Jansen JA, Postema PG, Nannenberg EA, Mizusawa Y, van der Nagel R, Wolswinkel R, van der Made I, Marchal GA, Rajamani S, et al. A common co-morbidity modulates disease expression and treatment efficacy in inherited cardiac sodium channelopathy. *Eur Heart J*. 2018;39:2898–2907.
8. Casini S, Verkerk AO, Remme CA. Human iPSC-derived cardiomyocytes for investigation of disease mechanisms and therapeutic strategies in inherited arrhythmia syndromes: strengths and limitations. *Cardiovasc Drugs Ther.* 2017;31:325–344.
9. Veerman CC, Kosmidis G, Mummery CL, Casini S, Verkerk AO, Bellin M. Immaturity of human stem-cell-derived cardiomyocytes in culture: fatal flaw or soluble Problem? *Stem Cells Dev*. 2015;24:1035–1052.
10. Portero V, Casini S, Hoekstra M, Verkerk AO, Mengarelli I, Belardinelli L, Rajamani S, Wilde AAM, Bezzina CR, Veldkamp MW, Remme CA. Anti-arrhythmic potential of the late sodium current inhibitor GS-458967 in murine *Scn5a*-1798insD$^{+/-}$ and human *SCN5A*-1795insD$^{+/-}$ iPSC-derived cardiomyocytes. *Cardiovasc Res*. 2017;113:829–838.
11. Meijer van Putten RME, Mengarelli I, Guan K, Zegers JG, van Ginneken ACG, Verkerk AO, Wilders R. Ion channelopathies in human induced pluripotent stem cell derived cardiomyocytes: a dynamic clamp study with virtual I_{K1}. *Front Physiol*. 2015;6:7.
12. Riedl A, Wawro N, Gieger C, Meisinger C, Peters A, Roden M, Kronenberg F, Herder C, Rathmann W, Völzke H, et al. Identification of Comprehensive Metabotypes Associated with Cardiometabolic Diseases in the Population-Based KORA Study. *Mol Nutr Food Res*. 2018;62:e1800117.

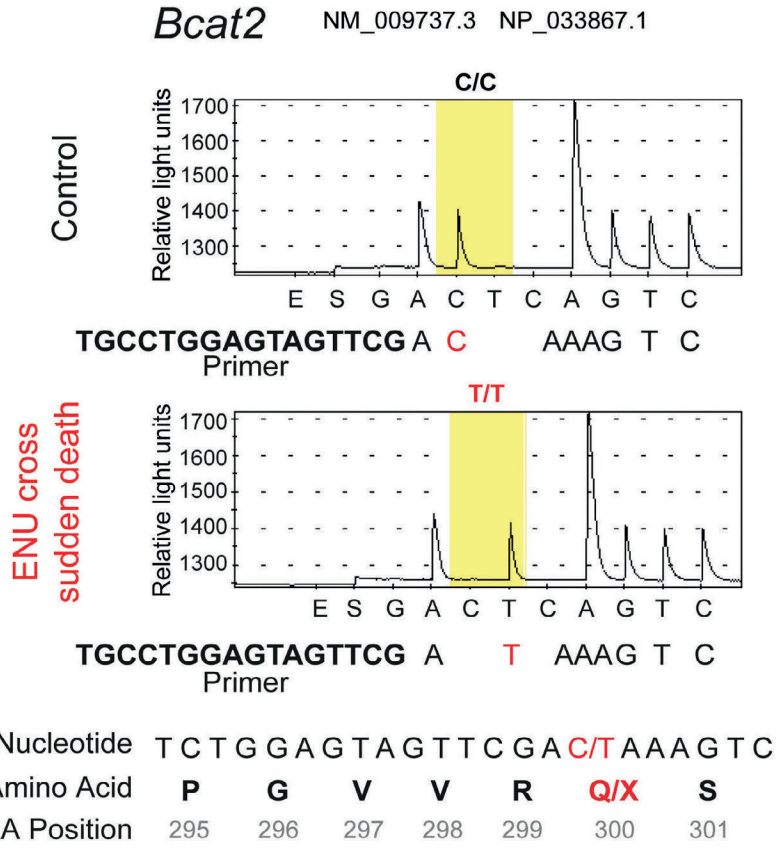

Supplemental Figure S1. Validation of the *Bcat2* variant identified in the initial G3 ENU screen.
Pyrosequencing confirmation of the ENU-induced mutation in Bcat2 showing the homozygous mutation in affected sudden death animals but absent from unaffected controls.

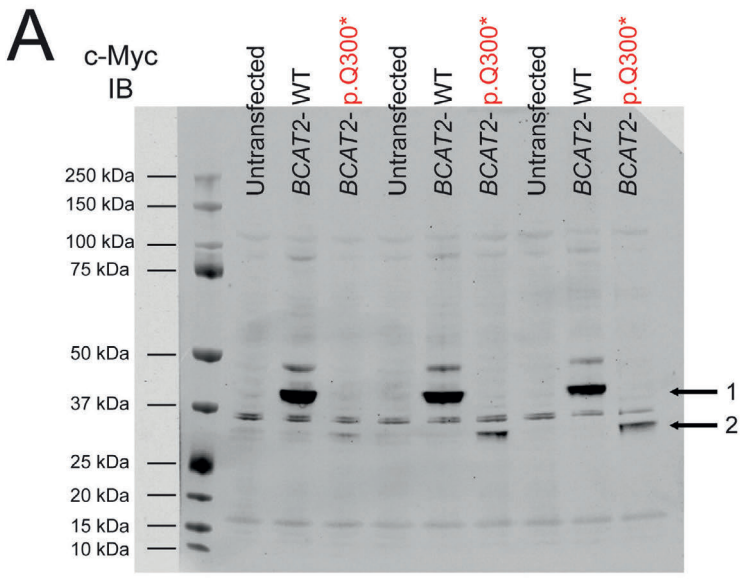

B

BCAT2: NP_033867.1

MAAATLGQVWARKLLPVPWLLCGSKRCVSSIFKAADLQIQMTKEPQKKPAP
SQALLFGKTFTDHMLMVEWNNKAGWGPPRIQPFQNLTLHPACSGLHYSLQL
FEGLKAYKGGDQQVRLFRPWLNMDRMLRSARRLCLPDFDKQELLECIRQLIEV
DKDWVPDGNGTSLYVRPVLIGNEPSLGVGMVTQALLYVILCPVGSYFPGDSM
TPVSLLADPSFVRAWIGGVGDCKLGGNYGPTVAVQREAQKRGCEQVLWLYGP
DHQLTEVGTMNIFVYWTHEDGVLELVTPPLNGVILPGVVRQSLLDLARTWGE
FRVAERKVTMKELKRALEEGRVREVFGSGTACQVCPVHQILYEGKQLHIPTME
NGPELILRFQKELKAIQYGASAHDWMFRV

1-27 - mitochondrial targeting sequence
Q - mutation
CQVC - CXXC motif important for catalysis (orientation of the substrate)
300-393 – deleted region

Supplemental Figure S2. Effect of the *BCAT2* ^{pQ300*} mutation on protein translation and predicted *BCAT2* protein sequence domains. (A) *BCAT2^{C1121T} transfected in HEK293 cells results in a truncated BCAT2 protein presenting with a smaller molecular weight (arrow 2) compared to BCAT2 WT (arrow 1).* **(B)** *BCAT2^{C1121T} is predicted to lack the CXXC catalytic motif essential for enzyme catalytic activity.*

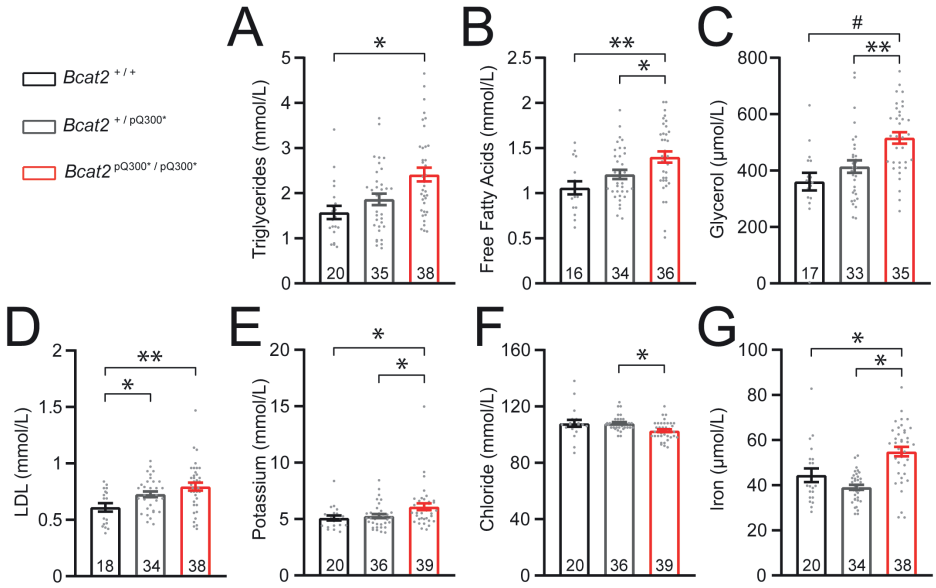

Supplemental Figure S3. Biochemical plasmatic analyses performed in mice from batch A from the initial ENU screen. *(**A**) Triglycerides (**B**) Free fatty acids (**C**) Glycerol (**D**) Low-density lipoproteins (LDL) (**E**) Potassium (**F**) Chloride (**G**) Iron. *P<0.05; **P≤0.01; #P≤0.001.*

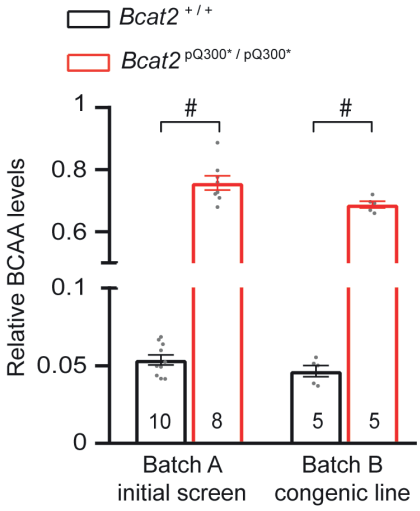

Supplemental Figure S4. Urinary relative BCAA quantification in the initial screen (batch A) and the congenic line (batch B) of *Bcat2*$^{p.Q300*/p.Q300*}$ mice. *Urinary BCAA levels (signal intensity from spectral region 1.08-0.90ppm), relative to signal intensity from spectral region 3.50-1.08ppm, from batch A (initial ENU screen) and batch B (backcrossed congenic line). #P≤0.001. The number of mice per grouping is summarised on the plot.*

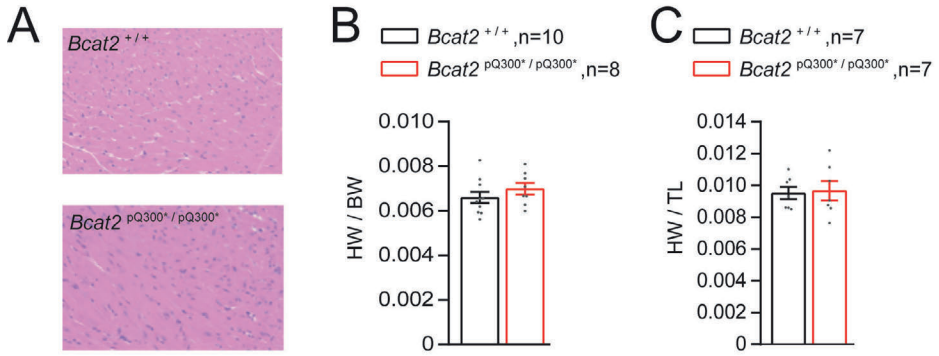

Supplemental Figure S5. Cardiac structural characterization of *Bcat2*$^{p.Q300*/p.Q300*}$ mice. (A) *Absence of fibrosis in hearts from Bcat2*$^{p.Q300*/p.Q300*}$ *mice; (***B***) Unchanged heart weight to body weight ratio and* **(C)** *heart weight to tibia length ratio in Bcat2*$^{p.Q300*/p.Q300*}$ *mice.*

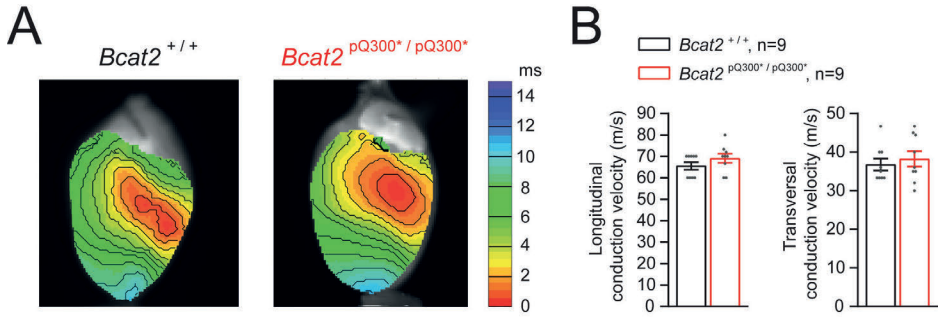

Supplemental Figure S6. Ventricular conduction velocity is unaffected in *Bcat2*$^{p.Q300*/p.Q300*}$ hearts. (A) *Typical examples of ventricular activation maps obtained with optical mapping on Langendorff perfused hearts.* **(B)** *Average values for longitudinal and transversal conduction velocities.*

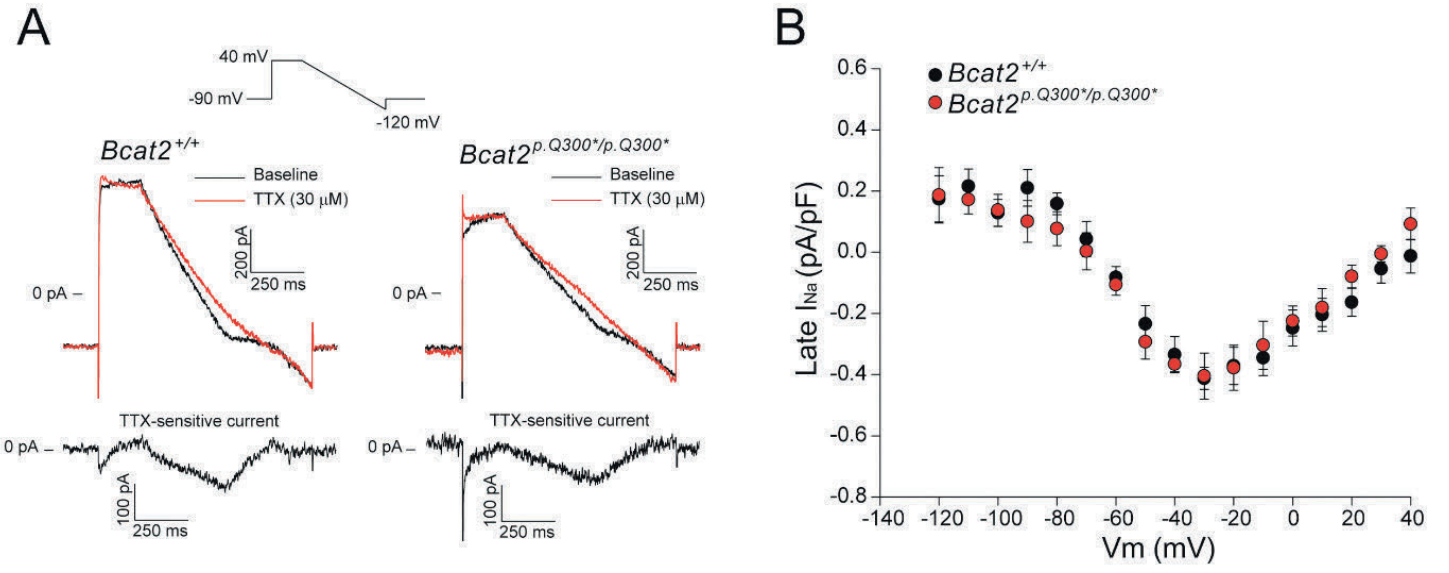

Supplemental Figure S7.

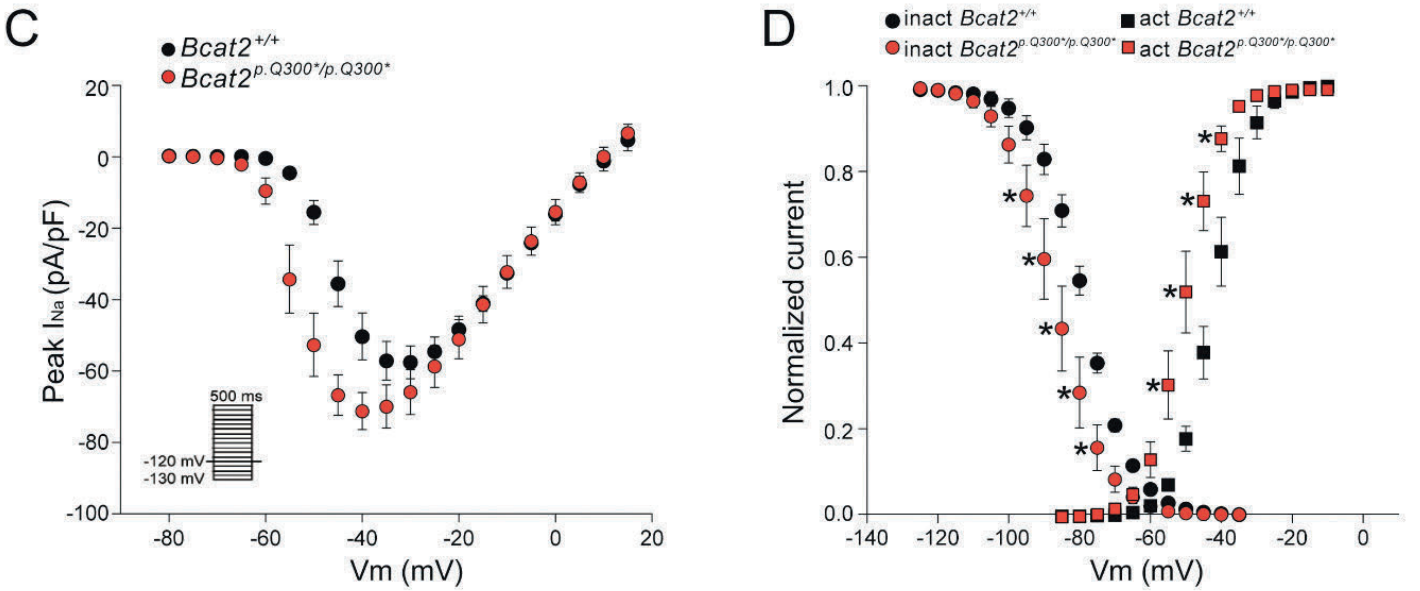

Supplemental Figure S7. Continued. *(**A**) Representative late sodium current (I_{Na}) traces recorded during a ramp protocol (inset) at baseline and after application of 30 µM tetrodotoxin (TTX). TTX -sensitive current was obtained by subtraction of the current recorded in the presence of TTX from the current recorded in the absence of the compound. (**B**) Average current-voltage (I-V) relationships for late I_{Na} measured as TTX- sensitive current shows no significant differences between Bcat2$^{+/+}$ (n=8) and Bcat2$^{p.Q300*/p.Q300*}$ (n=6) cardiomyocytes. (**C**) Average current-voltage (I-V) relationships for peak I_{Na} (protocol in inset) shows no significant differences between Bcat2$^{+/+}$ (n=4) and Bcat2$^{p.Q300*/p.Q300*}$ (n=5) cardiomyocytes. (**D**) Voltage dependence of activation and inactivation (*p<0.05). Average peak current densities and values for steady-state activation and inactivation are listed in Supplemental Table S4.*

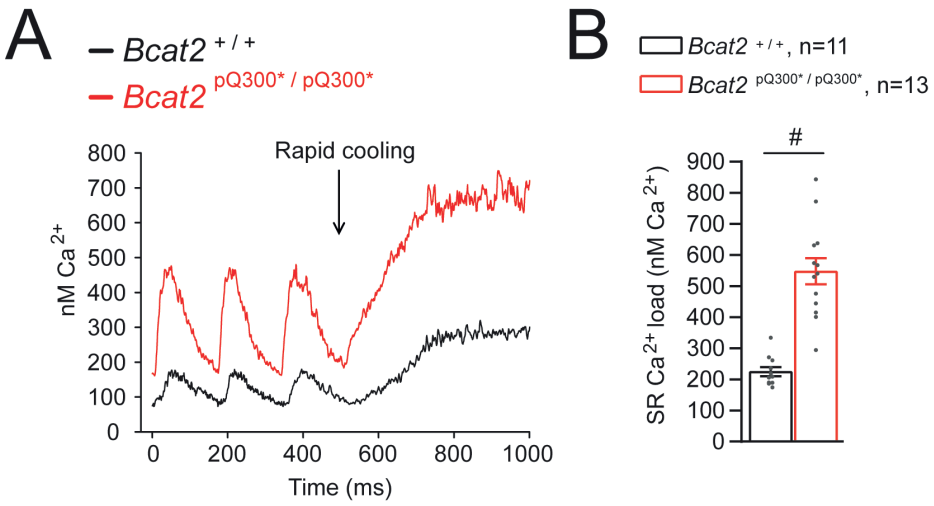

Supplemental Figure S8. Sarcoplasmic reticulum Ca^{2+} content and fast pacing induced Ca^{2+} transients in *Bcat2*$^{p.Q300*/p.Q300*}$ mice. **(A)** *Typical example of intracellular calcium recording after fast cooling enabling sarcoplasmic reticulum calcium content quantification triggered by rapid cooling in Bcat2*$^{p.Q300*/p.Q300*}$ *mice.* **(B)** *Average values of sarcoplasmic reticulum calcium content for both Bcat2*$^{+/+}$ *(n=11 cells from 6 mice) and Bcat2*$^{p.Q300*/p.Q300*}$ *(n=11 cells from 6 mice). #P≤0.001.*

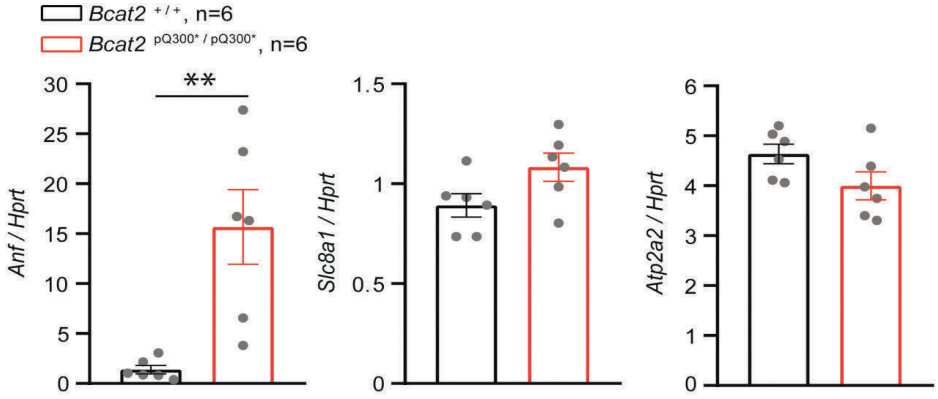

Supplemental Figure S9. mRNA expression levels in ventricular tissue of *Bcat2*$^{+/+}$ and *Bcat2*$^{p.Q300*/p.Q300*}$ mice of *Anf, Slc8a1* and *Atp2a2* (relative to *Hprt*).

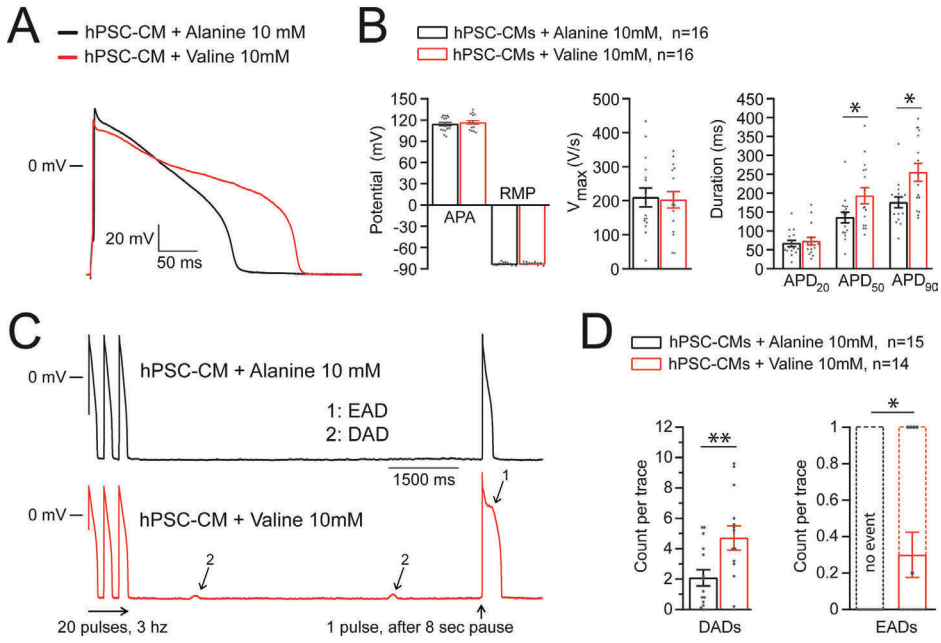

Supplemental Figure S10. Pro-arrhythmic effects of valine (10 mM) compared to alanine (10 mM) in human PSC derived cardiomyocytes (hPSC-CMs). **(A)** *Typical example of APs elicited at the stimulation frequency of 1Hz from hPSC-CMs incubated with medium containing 10 mM of alanine or with 10 mM valine.* **(B)** *Average values for APA (action potential amplitude), RMP (resting membrane potential), V_{max} (upstroke velocity) and APD (action potential duration) at 20%, 50% and 90% repolarization (APD_{20}, APD_{50}, APD_{90}) of hPSC-CMs incubated with either 10 mM alanine medium (n=16), or 10 mM valine medium (n=16).* **(C)** *Typical examples of EADs (1) and DADs (2) recorded after a fast pacing stimulation protocol (20 pulses at 3-Hz followed by a 8s pause and 1 pulse followed by a 1s pause).* **(D)** *Average count per trace for DADs and EADs observed in hPSC-CMs incubated with 10 mM alanine (n=15) and 10 mM valine (n=14) medium. *P<0.05; **P≤0.01.*

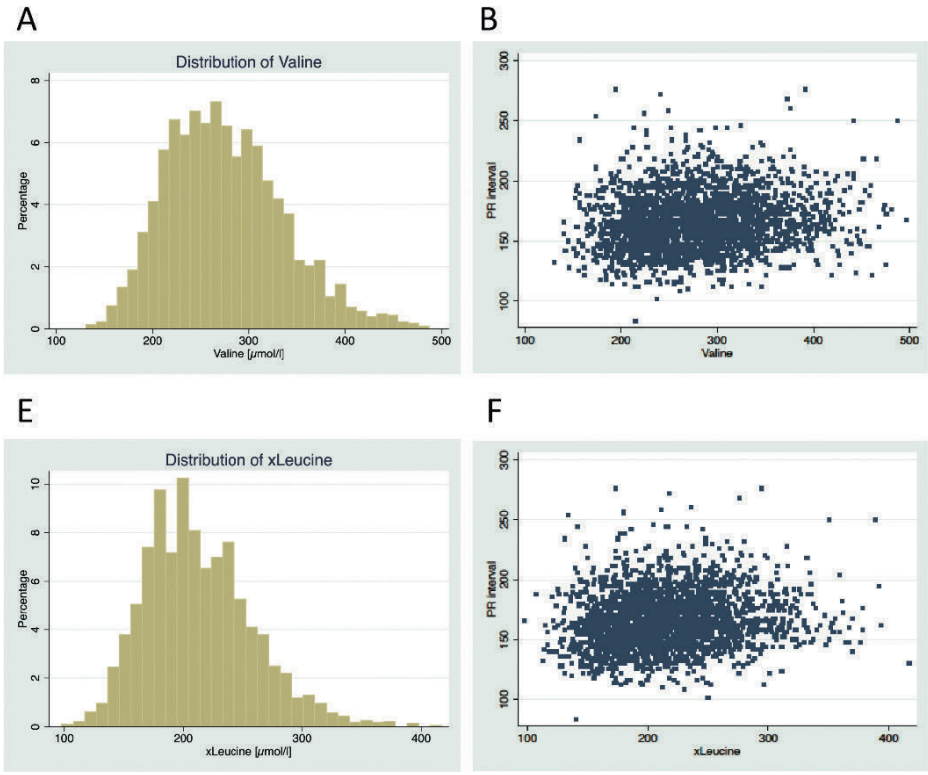

Supplemental Figure 11. The distribution of BCAAs in the KORA F4 cohort and their relation with ECG measures. .

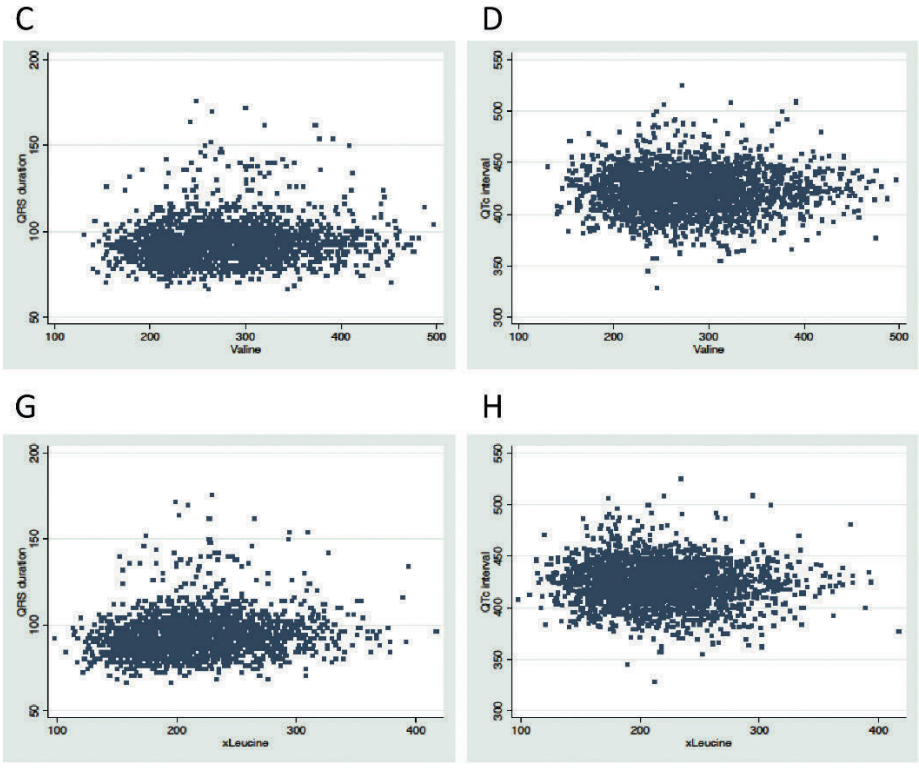

Supplemental Figure 11. Continued. *The upper row shows valine results, the lower row shows xleucine results. Panels **A** and E, respectively, visualize the distribution of valine and xleucine, respectively. The remaining panels indicate a linear relation of the PR interval (panels **B** and **F**), the QRS duration (panels **C** and **G**), and the QTc interval (panels **D** and **H**) with valine and xleucine, respectively. The PR, QRS and QTc interval values are expressed in ms. BCAA concentrations are expressed in µmol/L.*

Supplementary Table S1: List of parameters measured in the plasma clinical chemistry screen.

Parameter	Units	Parameter	Units
Sodium	(mmol/L)	LDL	(mmol/L)
Potassium	(mmol/L)	Glucose	(mmol/L)
Chloride	(mmol/L)	Triglycerides	(mmol/L)
Urea	(mmol/L)	Glycerol	(µmol/L)
Creatinine	(µmol/L)	Free Fatty Acids	(mmol/L)
Calcium	(mmol/L)	Total Billirubin	(µmol/L)
Inorganic Phosphorus	(mmol/L)	LDH	(U/L)
ALP	(U/L)	Iron	(µmol/L)
ALT	(U/L)	Amylase	(U/L)
AST	(U/L)	Creatine Kinase	(U/L)
Total Protein	(g/L)	Uric Acid	(µmol/L)
Albumin	(g/L)	Ketone Bodies	(mmol/L)
Total Cholesterol	(mmol/L)	Fructose	(µmol/L)
HDL	(mmol/L)	Magnesium	(mmol/L)

Supplemental Table S2: Values and statistics of measurements from *Bcat2*$^{+/+}$ and *Bcat2*$^{pQ300*/pQ300*}$ mice and hearts.

	n	*Bcat2* $^{+/+}$	n	*Bcat2*$^{p.Q300*/p.Q300*}$	Statistical test	P value
HW / BW	10	0.0066 ± 0.0003	8	0.0069 ± 0.0002	t-test	P = 0.300
HW / TL	7	0.0095 ± 0.0006	7	0.0096 ± 0.0004	t-test	P = 0.838
qPCR *Anf / Hprt*	6	1.39 ± 0.41	6	15.67 ± 3.74	Mann-Whitney Rank sum test	P = 0.002
qPCR *Slc8a1 / Hprt*	6	0.89 ± 0.06	6	1.08 ± 0.08	t-test	P = 0.063
qPCR *Atp2a2 / Hprt*	6	4.64 ± 0.2	6	4 ± 0.28	t-test	P = 0.091
mTOR total (relative to GAPDH)	7	1 ± 0.07	6	1.79 ± 0.33	Mann-Whitney Rank sum test	P = 0.035
P-mTOR (relative to GAPDH)	7	1 ± 0.15	6	4.06 ± 0.92	Mann-Whitney Rank sum test	P = 0.002

Supplemental Table S2: Continued.

	n	*Bcat2* $^{+/+}$	n	*Bcat2* $^{p.Q300*/p.Q300*}$	Statistical test	P value
Ratio p-mTOR/ mTOR total	7	1 ± 0.14	6	2.62 ± 0.61	t-test	P = 0.017
Heart rate (beat/min)	11	491.6 ± 14.1	15	505.1 ± 9.7	t-test	P = 0.420
QRS interval (ms)	11	10.5 ± 0.2	15	11.2 ± 0.1	t-test	P = 0.121
PR interval (ms)	11	35.3 ± 0.9	15	38.7 ± 0.4	t-test	P ≤ 0.001
QT interval (ms)	11	44.8 ± 1.2	15	48.7 ± 1.1	t-test	P ≤ 0.05
QTc interval (ms)	11	40.4 ± 0.8	15	44.6 ± 0.8	t-test	P ≤ 0.001
Transversal CV (m/s)	9	37.8 ± 1.5	9	38.2 ± 2.0	t-test	P = 0.573
Longitudinal CV (m/s)	9	65.6 ± 1.8	9	69.1 ± 2.1	t-test	P = 0.213
APD_{70} (optical) (ms)	7	43.9 ± 3.1	7	60.4 ± 6.0	Mann-Whitney Rank sum test	P = 0.038
Longest minus shortest APD_{70} (optical) (ms)	7	9.1 ± 1.3	7	16.3 ± 1.9	t-test	P = 0.013

Supplemental Table S3: Plasma clinical chemistry results and statistics in *Bcat2* $^{+/+}$ and *Bcat2* $^{pQ300*/pQ300*}$ mice.

Murine model	n	*Bcat2* $^{+/+}$	n	*Bcat2* $^{+/p.Q300*}$	n	*Bcat2* $^{p.Q300*/p.Q300*}$	Statistical test and P value
Triglyceride (mmol/L)	20	1.57 ± 0.14	35	1.86 ± 0.12	38	2.41 ± 0.15	1 way anova on ranks – Dunn's method - WT vs Homozygous: P value <0.05
Free fatty acids (mmol/L)	16	1.05 ± 0.07	34	1.20 ± 0.05	36	1.40 ± 0.06	Student-Newman-Keuls Method - WT vs Homozygous: P value <0.05 (0.003) -Heterozygous vs homozygous: P value <0.05 (0.016)
Glycerol (µmol/L)	17	360.9 ± 31.2	33	414.3 ± 21.7	35	516.1 ± 20.4	Student-Newman-Keuls Method - WT vs Homozygous: P value <0.001 -Heterozygous vs homozygous: P < 0.001
LDL (mmol/L)	20	0.61 ±0.04	35	0.72 ± 0.02	39	0.79 ± 0.03	Student-Newman-Keuls Method - WT vs Heterozygous: P <0.05 (0.029) - WT vs Homozygous: P <0.01 (0.002)
Potassium (mmol/L)	20	5.1 ± 0.2	36	5.3 ± 0.2	39	6.1 ± 0.3	1 way anova on ranks – Dunn's method - WT vs Homozygous: P <0.05 Homozygous vs heterozygous: P <0.05
Chloride (mmol/L)	20	107.9 ± 2.5	36	107.9± 0.9	39	102.7 ± 1.0	1 way anova on ranks – Dunn's method - Heterozygous vs homozygous: P <0.05

Supplemental Table S3: Continued.

Murine model	n	*Bcat2* $^{+/+}$	n	*Bcat2* $^{+/p.Q300*}$	n	*Bcat2* $^{p.Q300*/p.Q300*}$	Statistical test and P value
Iron (µmol/L)	20	44.4 ± 3.0	34	39.1 ± 1.2	38	54.9 ± 2.1	1 way anova on ranks – Dunn's method - WT vs homozygous: P value <0.05 - Heterozygous vs homozygous: P <0.05
BCAAs (mmol/L)	11	1.83 ± 0.1	9	2.05 ± 0.2	7	19.6 ± 2.8	1 way anova on ranks – Dunn's method - WT vs homozygous: P <0.05 - Heterozygous vs homozygous: P <0.05
Valine (mmol/L)	11	0.55 ± 0.03	9	0.68 ± 0.03	7	9.9 ± 0.54	1 way anova on ranks – Dunn's method - WT vs homozygous: P <0.05
xLeucine (mmol/L)	11	1.6 ± 0.09	9	1.7 ± 0.06	7	10.2 ± 0.49	1 way anova on ranks – Dunn's method - WT vs homozygous: P <0.05 - Heterozygous vs homozygous: P <0.05

Supplemental Table S4. Values and statistics of patch clamp measurements in isolated cardiomyocytes from *Bcat2*$^{+/+}$ and *Bcat2* $^{pQ300*/pQ300*}$ mice.

	n	*Bcat2* $^{+/+}$	n	*Bcat2* p.Q300*/p.Q300*	Statistical test	P value
Action potentials						
APA (mV)	13	112.4± 1.8	7	117.2 ±1.4	t-test	P = 0.093
RMP (mV)	13	-85.9 ± 0.6	7	-85.5 ± 0.7	t-test	P = 0.713
V_{max} (V/s)	13	509.5 ± 42.9	7	654.0 ± 39.9	t-test	P = 0.041
APD_{20}	13	0.83 ± 0.08	7	0.86 ± 0.15	t-test	P = 0.856
APD_{50}	13	2.29 ± 0.31	7	2.95 ± 0.78	Mann-Whitney Rank sum test	P = 0.905
APD_{90}	13	88.5 ± 5.8	7	116.8 ± 8.7	t-test	P = 0.01
Sodium current (I_{Na})						
Peak I_{Na} density at -20 mV (pA/pF)	4	-48.4 ± 3.7	5	-51.1 ± 5.5	t-test	P = 0.706
Steady-state activation $V_{1/2}$ (mV)	4	-42.7 ± 2.1	5	-50.2 ± 1.9	t-test	P = 0.036
Steady-state activation *k* (mV)	4	4.8 ± 0.3	5	4.5 ± 0.2	t-test	P = 0.413
Steady-state inactivation $V_{1/2}$ (mV)	4	-79.4 ± 1.0	5	-86.4 ± 2.7	t-test	P = 0.059
Steady-state inactivation *k* (mV)	4	6.9 ± 0.4	5	6.3 ± 0.1	t-test	P = 0.186
Late I_{Na} density at -20 mV (pA/pF)	8	-0.37 ± 0.06	6	-0.38 ± 0.06	t-test	P=NS

APA (action potential amplitude); RMP (resting membrane potential); V_{max} (upstroke velocity); APD (action potential duration) at 20%, 50% and 90% repolarization (APD_{20}, APD_{50}, APD_{90}); $V_{1/2}$ (membrane potential for the half-maximal (in)activation); k (slope factor).

Supplemental Table S5. Values and statistics of intracellular calcium measurements in isolated cardiomyocytes from *Bcat2*$^{+/+}$ and *Bcat2* $^{pQ300*/pQ300*}$ mice.

	n	*Bcat2* $^{+/+}$	n	*Bcat2* $^{p.Q300*/p.Q300*}$	Statistical test	P value
Diastolic Ca^{2+} (nmol/L)	12	75.3 ± 8.5	17	162.8 ± 12	t-test	P ≤ 0.001
Peak Ca^{2+} transient (nmol/L)	12	171.3 ± 15.5	17	468.6 ± 48.1	Mann-Whitney Rank sum test	P ≤ 0.001
Ca^{2+} transient amplitude (nmol/L)	12	96.0 ± 11.6	17	305.8 ± 39.6	Mann-Whitney Rank sum test	P ≤ 0.001
Ca^{2+} transient decay (ms)	9	73.7 ± 7.9	12	71.3 ± 6.6	t-test	P = 0.813
Diastolic Ca^{2+} (nmol/L) -Noradrenaline (50 nmol/L)	9	110.0 ± 18.8	14	142.0 ± 18.7	t-test	P = 0.258
Systolic Ca^{2+} (nmol/L) - Noradrenaline (50 nmol/L)	9	424.2 ± 62.6	14	584.3 ± 126.3	Mann-Whitney Rank sum test	P = 0.474
Ca^{2+} transient amplitude (nmol/L) - Noradrenaline (50 nmol/L)	9	314.2 ± 47.5	14	442.3 ± 113.4	Mann-Whitney Rank sum test	P = 0.633
Ca^{2+} transient decay (ms) – Noradrenaline (50 nmol/L)	9	47.8 ± 4.2	13	44.7 ± 2.1	t-test	P = 0.479
Diastolic Ca^{2+} (nM) following rapid cooling	11	62.7 ± 6.3	13	153.4 ± 13.0	t-test`	P ≤ 0.001
Peak Ca^{2+} (nM) following rapid cooling	11	287.7 ± 16.3	13	701.5 ± 47.3	Mann-Whitney Rank sum test	P ≤ 0.001
SR Ca^{2+} load (nM) following rapid cooling	11	225.0 ± 14.4	13	548.0 ± 41.9	Mann-Whitney Rank sum test	P ≤ 0.001

Supplemental Table S5. Continued.

	n	*Bcat2* $^{+/+}$	n	*Bcat2* $^{p.Q300*/p.Q300*}$	Statistical test	P value
Ratio diastolic/peak Ca^{2+} following rapid cooling	11	4.9 ± 0.4	13	4.9 ± 0.4	t-test	P = 0.994
Non-triggered AP Ca^{2+} after-transients (count/trace)	9	1.9 ± 0.8	15	4.3 ± 0.9	Mann-Whitney Rank sum test	P = 0.064
Triggered AP Ca^{2+} after-transients (count/trace)	9	0.4 ± 0.3	15	4.6 ± 0.6	Mann-Whitney Rank sum test	P = 0.393
Total Ca^{2+} after-transients (count/trace)	9	2.3 ± 0.7	15	5.5 ± 1.0	t-test	P = 0.034
Non-triggered AP Ca^{2+} after-transients (count/trace) – Noradrenaline (50 nmol/L)	9	4.0 ± 0.8	10	4.8 ± 1.3	t-test	P = 0.611
Triggered AP Ca^{2+} after-transients (count/trace) – Noradrenaline (50 nmol/L)	9	0.6 ± 0.6	10	6.6 ± 3.0	Mann-Whitney Rank sum test	P = 0.012
Total Ca^{2+} after-transients (count/trace) – Noradrenaline (50 nmol/L)	9	4.6 ± 0.7	10	11.4 ± 3.7	Mann-Whitney Rank sum test	P = 0.004

Supplemental Table S6: Effect of BCAAs and combination of BCAAs and rapamycin 500 nmol/L on hPSC-CM electrophysiological properties

hPSC-CMs	n	CTL medium	n	BCAAs	n	BCAAs + Rapamycin	Statistical test P value
RMP (mV)	25	-83.04 ± 0.35	25	-83.19 ± 0.38	24	-82.93 ± 0.47	1-way ANOVA on ranks – Dunn's method NS (Ranks)
APA (mV)	25	111.51 ± 2.02	25	115.26 ± 1.39	24	106.67 ± 2.01	1-way ANOVA on ranks – Dunn's method NS
V_{max} (V/s)	25	170.27 ± 28.22	25	184.96 ± 23.81	24	173.23 ± 16.45	1-way ANOVA NS
APD_{20} (ms)	25	69.12 ±0.7	25	71.73 ± 5.74	24	52.82 ± 6.87	1-way ANOVA NS
APD_{50} (ms)	25	143.68 ± 12.1	25	191.1 ± 21.06	24	141.42 ± 15.74	1-way ANOVA on ranks – Dunn's method NS
APD_{90} (ms)	25	190.75 ± 14.16	25	256.51 ± 21.71	24	199.15 ± 16.46	Student-Newman-Keuls Method -- CTL vs BCAAs: P <0.05 - BCAAs vs BCAAs+ rapa: P <0.05
DADs (Count per trace)	23	2.7 ± 0.63	24	5.37 ± 0.59	19	2.66 ± 0.57	1-way ANOVA on ranks – Dunn's method - CTL vs BCAAs: P <0.05 - BCAAs vs BCAAs+ rapa: P <0.05
EADs (Count per trace)	23	0	24	0.38 ± 0.1	19	0	1-way ANOVA on ranks – Dunn's method -CTL vs BCAAs: P <0.05 - BCAAs vs BCAAs + rapa: P <0.05

Supplemental Table S6: Continued.

hPSC-CMs	n	CTL medium	n	BCAAs	n	BCAAs + Rapamycin	Statistical test P value
Diastolic Ca^{2+} (nM)	22	73.62 ± 7.96	24	147.53 ± 16.47	22	93.98 ± 11.86	1-way ANOVA on ranks – Dunn's method -CTL vs BCAAs: P <0.05 - BCAAs vs BCAAs + rapa: P <0.05
Peak transient (nM)	22	182.64 ± 15.42	24	312.67 ± 24.29	22	187.29 ± 21.48	1-way ANOVA on ranks – Dunn's method -CTL vs BCAAs: P <0.001 - BCAAs vs BCAAs + rapa: P <0.001
Transient amplitude (nM)	22	105.29 ± 10.54	24	166.93 ± 11.48	22	93.31 ± 14.48	1-way ANOVA on ranks – Dunn's method -CTL vs BCAAs: P <0.05 - BCAAs vs BCAAs + rapa: P <0.05
Non-triggered AP Ca^{2+} transient (EC/T)	17	1 ± 0.4	16	4 ± 1.39	14	1 ± 0.72	1-way ANOVA on ranks NS
Triggered AP Ca^{2+} transient (EC/T)	17	1 ± 0.27	16	2 ± 0.71	14	1 ± 0.37	1-way ANOVA on ranks NS
Total Ca^{2+} transient (EC/T)	17	2 ± 0.41	16	6 ± 1.32	14	2 ± 0.76	1-way ANOVA on ranks – Dunn's method -CTL vs BCAAs: P <0.05 - BCAAs vs BCAAs + rapa: P <0.05

APA (action potential amplitude); RMP (resting membrane potential); V_{max} (upstroke velocity); APD (action potential duration) at 20%, 50% and 90% repolarization (APD_{20}, APD_{50}, APD_{90}); EADs (early afterdepolarizations); DADs (delayed afterdepolarizations).

Supplemental Table S7: Effect of rapamycin 500 nmol/L on hPSC-CMs electrophysiological properties.

hPSC-CMs	n	CTL medium	n	CTL medium + Rapamycin	Statistical test
RMP (mV)	25	-83.04 ± 0.35	11	-83.50 ± 0.93	Mann-Whitney Rank sum test NS
APA (mV)	25	111.51 ± 2.02	11	108.38 ± 2.84	Mann-Whitney Rank sum test NS
V_{max} (V/s)	25	170.27 ± 28.22	11	190.07 ± 23.23	t-test NS
APD_{20} (ms)	25	69.12 ±0.7	11	77.19 ± 12.63	t-test NS
APD_{50} (ms)	25	143.68 ± 12.1	11	155.17 ± 22.63	t-test NS
APD_{90} (ms)	25	190.75 ± 14.16	11	204.21 ± 20.2	t-test NS
DADs (Count per trace)	23	2.7 ± 0.63	9	0.99 ± 0.34	Mann-Whitney Rank sum test NS
EADs (Count per trace)	23	0	9	0	Not tested No events recorded

APA (action potential amplitude); RMP (resting membrane potential); V_{max} (upstroke velocity); APD (action potential duration) at 20%, 50% and 90% repolarization (APD_{20}, APD_{50}, APD_{90}); EADs (early afterdepolarizations); DADs (delayed afterdepolarizations).

Supplementary Table S8. Effect of valine 10 mmol/l compared to alanine 10 mmol/l on hPSC-CMs electrophysiological properties.

hPSC-CMs	n	Alanine 10mM	n	Valine 10mM	Statistical test
RMP (mV)	16	-83 ± 0.48	16	-82.53 ± 0.42	t-test NS
APA (mV)	16	114.26 ± 2.57	16	116.8 ± 2.6	Mann-Whitney Rank sum test NS
V_{max} (V/s)	16	209.97 ± 27.56	16	202.66 ± 24.32	t-test NS
APD_{20} (ms)	16	66.82 ± 8.02	16	72.88 ± 10.13	Mann-Whitney Rank sum test NS
APD_{50} (ms)	16	135.46 ± 14.05	16	193.03 ± 21.54	t-test P = 0.033

Supplementary Table S8. Continued.

hPSC-CMs	n	Alanine 10mM	n	Valine 10mM	Statistical test
APD_{90} (ms)	16	175.2 ± 14.28	16	254.89 ± 23.87	Mann-Whitney Rank sum test P = 0.025
DADs (Count per trace)	15	2.09 ± 0.53	14	4.71 ± 0.8	t-test P = 0.01
EADs (Count per trace)	15	0	14	0.3 ± 0.12	Mann-Whitney Rank sum test P= 0.014

APA (action potential amplitude); RMP (resting membrane potential); V_{max} (upstroke velocity); APD (action potential duration) at 20%, 50% and 90% repolarization (APD_{20}, APD_{50}, APD_{90}); EADs (early afterdepolarizations); DADs (delayed afterdepolarizations).

Supplementary Table S9. Surface ECG parameters in male and female *Bcat2* $^{+/+}$ and *Bcat2p*$^{p.Q300*/p.Q300*}$ mice.

Murine model	n	*Bcat2* $^{+/+}$	n	*Bcat2*$^{p.Q300*/p.Q300*}$	Statistical test	P value
Males						
Heart rate (beat/min)	6	474.6 ± 22.1	8	512.2 ± 14.0	t-test	P = 0.129
QRS interval (ms)	6	10.2 ± 0.5	8	11.5 ± 0.5	t-test	P = 0.039
PR interval (ms)	6	34.7 ± 1.2	8	38.1 ± 0.6	t-test	P = 0.009
QT interval (ms)	6	44.5 ± 1.7	8	48.2 ± 1.6	t-test	P = 0.120
QTc interval (ms)	6	39.4 ± 0.6	8	44.4 ± 1.3	t-test	P = 0.005
Females						
Heart rate (beat/min)	5	511.9 ± 19.2	7	497.1 ± 16.0	t-test	P = 0.530
QRS interval (ms)	5	10.8 ± 0.4	7	10.8 ± 0.5	t-test	P = 0.969
PR interval (ms)	5	36.0 ± 1.6	7	39.4 ± 0.6	t-test	P = 0.037
QT interval (ms)	5	45.2 ± 2.4	7	49.4 ± 1.9	t-test	P = 0.159
QTc interval (ms)	5	41.7 ± 1.7	7	44.8 ± 1.2	t-test	P = 0.130